Title

Immune perturbations in human pancreas lymphatic tissues prior to and after type 1 diabetes onset

Authors

Gregory J. Golden[1,2], Vincent H. Wu[1,2], Jacob T. Hamilton[1,2], Kevin R. Amses[1], Melanie R. Shapiro[3], Alberto Sada Japp[1,2], Chengyang Liu[2,4], Maria Betina Pampena[1,2], Leticia Kuri-Cervantes[1,2], James J. Knox[2,5], Jay S. Gardner[1,2], HPAP Consortium[6], Mark A. Atkinson[3,7], Todd M. Brusko[3,7,8], Eline T. Luning Prak[2,5], Klaus H. Kaestner[9], Ali Naji[2,4], Michael R. Betts[1,2,10]*

Affiliations

[1]Department of Microbiology, University of Pennsylvania, Perelman School of Medicine, Philadelphia, PA 19104, USA

[2]Institute for Immunology, University of Pennsylvania, Perelman School of Medicine, Philadelphia, PA 19104, USA

[3]Department of Pathology, Immunology and Laboratory Medicine, University of Florida Diabetes Institute, College of Medicine, Gainesville, FL 32610, USA

[4]Department of Surgery, University of Pennsylvania, Perelman School of Medicine, Philadelphia, PA 19104, USA

[5]Department of Pathology and Laboratory Medicine, University of Pennsylvania, Perelman School of Medicine, Philadelphia, PA 19104, USA

[6]The Human Pancreas Analysis Program, Perelman School of Medicine, Philadelphia, PA 19104, USA

[7]Department of Pediatrics, College of Medicine, University of Florida, Gainesville, FL 32610, USA

[8]Department of Biochemistry and Molecular Biology, College of Medicine, University of Florida, Gainesville, FL 32610, USA

[9]Department of Genetics and Institute for Diabetes, Obesity, and Metabolism, University of Pennsylvania, Perelman School of Medicine, Philadelphia, PA 19104, USA

[10]Lead Contact

*Correspondence: betts@pennmedicine.upenn.edu (M.R.B.)

Keywords

Type 1 diabetes, pancreatic lymph node, mesenteric lymph node, spleen, flow cytometry, CITEseq

Abstract

Autoimmune destruction of pancreatic β cells results in type 1 diabetes (T1D), with pancreatic immune infiltrate representing a key feature in this process. Studies of human T1D immunobiology have predominantly focused on circulating immune cells in the blood, while mouse models suggest diabetogenic lymphocytes primarily reside in pancreas-draining lymph nodes (pLN). A comprehensive study of immune cells in human T1D was conducted using pancreas draining lymphatic tissues, including pLN and mesenteric lymph nodes (mLN), and the spleen from non-diabetic control, β cell autoantibody positive non-diabetic (AAb+), and T1D organ donors using complementary approaches of high parameter flow cytometry and CITEseq. Immune perturbations suggestive of a proinflammatory environment were specific for T1D pLN and AAb+ pLN. Compared to ND, AAb+ and T1D pLN have a reduced Treg signature and increased stem-like *CXCR3*+*GZMK*-*TOX*- CD8+ T cells. Several perturbations in the pLN were T1D specific, including a reduced naive T cell signature and an increased frequency of cytotoxic CD56dimCD16+ NK cells. Some, but not all, immune changes were found in the mLN and spleen. In addition, certain immune populations correlated with high T1D genetic risk independent of disease state. These datasets form an extensive resource for profiling human lymphatic tissue immune cells in the context of autoimmunity and T1D.

Introduction

Type 1 diabetes (T1D) results in life long exogenous insulin dependence following autoimmune destruction of pancreatic islet β cells[1]. While β cell autoimmunity may start beforehand as suggested by the appearance of β cell-specific autoantibodies (AAb), the disease can take years to progress to overt hyperglycemia[2]. Evidence of β cell mass and insulin secretion can be detected even in long-standing T1D patients[3,4], with clinically beneficial effects associated with residual β cell function[5]. T1D genetic risk is primarily associated with human leukocyte antigen (HLA) loci but also with genes involved in regulating immune responses[2,6–8]. Accordingly, T cell anergy-inducing immunotherapy shows efficacy in individuals at risk for imminent T1D onset but only delays T1D onset by ~24 months[9,10]. The development of therapies capable of halting autoimmune progression and preserving β cell function requires further understanding of the complex immune cell responses that occur pre- and post-T1D diagnosis.

Human immunophenotypes associated with T1D include T cell[11–13], B cell[14,15], and natural killer (NK) cell[16] perturbations as well as accelerated immunological aging[17] in peripheral blood mononuclear cells (PBMCs). While surveying PBMCs can be informative, the immune system operates primarily within tissue microenvironments and disease-specific signatures may not be fully recapitulated in circulating immune cells [18–22]. Indeed, pancreatic islets of T1D individuals contain β cell antigen-specific CD8+ T cells[23], and the frequency of CD8+ T cells that recognize β cell antigens in the pancreas, not the blood, distinguishes T1D from healthy donors[24]. Surveying immunophenotypes in the pancreas itself has greatly increased our understanding of T1D pathogenesis[25–30]; however, the immunological processes that occur in pancreas-draining lymphoid tissues that may initiate or exacerbate T1D development and progression remain largely unclear.

Evidence suggests that pancreatic lymph nodes (pLNs) harbor immune cells that participate in T1D autoimmunity[31–34]. Studies in the non-obese diabetic (NOD) mouse model of T1D suggest that pLN lymphadenectomy early in autoimmune development protects against diabetes[31]. Further, pLNs in the mouse model contain stem-like β cell-specific memory CD8+ T cells, which seed cytotoxic and terminally-differentiated effector cells that traffic to the pancreas and eliminate β cells[34]. In humans, pLN from T1D donors contain insulin peptide-reactive T cells[32], and are enriched for β cell antigen-reactive T cell receptor (TCR) clones[33]. pLN from T1D donors also contain phenotypic alterations that suggest a more proinflammatory T cell population, specifically increased frequencies of Th17 effector CD4+ T cells with reciprocal decreases in regulatory T cell (Treg) and follicular regulatory T cell frequencies[35,36]. While these observations implicate the pLN as a hub of T1D autoimmunity, due to the rarity of these sample types, there has not been a comprehensive unbiased analysis of human pLN that effectively captures this immune environment.

To address these knowledge gaps, we profiled lymphoid immune perturbations across T1D autoimmune development within pLNs, mesenteric lymph nodes (mLNs), and spleen from control non-diabetic autoantibody negative (ND), non-diabetic AAb+, and T1D donors. We performed deep immunophenotyping of these tissues using high-parameter flow cytometry (n = 46 donors) and cellular indexing of transcriptomes and epitopes by sequencing (CITEseq; n = 18 donors). Taken together, our findings reveal novel immunophenotypes in pLN and mLN from both AAb+ and T1D donors that provide new insights into T1D pathogenesis.

Results

Immune profiling of pancreatic, mesenteric, and splenic lymphatic tissues

Through the Human Pancreas Analysis Program (HPAP)[37], we collected age, race, and sex matched ND, AAb+, and T1D donor spleens, and lymph nodes that drain the pancreas, including pLNs (pancreatic head, body, and tail) and mLNs (superior mesenteric artery termed SMA mLN, and upper mesentery termed MES mLN). We used two complementary techniques for deep immune cell profiling of these tissues: high-parameter flow cytometry on 256 unique samples (18 ND, 10 AAb+, and 18 T1D donors, Table S1) and CITEseq single cell analysis on 650,085 cells post quality control (6 ND, 5 AAb+, and 7 T1D donors, Table S2). All data are publicly available on PANC-DB (https://hpap.pmacs.upenn.edu/) or Genbank (GSE221787).

We first used a high parameter flow cytometry panel to assess inter-tissue immune differences amongst all major immune cell populations across several immune lineages, including T cells, B cells, innate cells, and subsets thereof (Figure 1A-C, S1). The spleen showed a unique immune profile compared to LNs (Figure 1A-E), with an increased frequency of NK cells (Figure S2A), monocytes, and CCR7- T cell subsets including effector memory (Tem) and Tem CD45RA+ (Temra) T cells (Figure 1C,E). Some subsets were evenly distributed across the spleen and LNs, including B cells (Figure 1C, S2B). In contrast, the LNs were enriched for T cells, particularly CD4+ T cells and naive T cell subsets (Figure 1C-E, S2C-D). The pLNs and mLNs were highly similar in immune cell composition, with few exceptions (Figure S2E-I). Innate lymphoid cells (ILCs) were slightly decreased in frequency within the MES mLN (Figure S2E), CD8+ central memory T cells (Tcm) had a slightly higher frequency occurring in the pLN-Tail (Figure S2F), and NK cells had a slightly decreased frequency in the pLN-Tail (Figure S2A).

In parallel, we performed CITEseq on a subgroup of the same donors, allowing for deep resolution of immune subsets in pLN, mLN, and spleen samples (Figure 1F). No specific immune population selectively resolved by disease state (Figure 1G). Major clusters identified include B cells, T cells, and innate immune cells (Figure 1H), with surface epitopes (Figure S3A) and gene transcripts (Figure S3B) defining subsets thereof. Some clusters in B and T cells contain over 30,000 cells, with at least a few hundred cells in less abundant populations, allowing for deep characterization of rare immune cell populations of interest (Figure 1I). The spleen contained the majority of innate immune cells, while the pLN and mLN samples contained the majority of T cells (Figure 1F,H,I), closely resembling the flow cytometry dataset.

AAb+ and T1D associated shifts in immune phenotypes

To define immune cell composition and phenotypic changes in T1D development, we compared immune cell population frequencies between ND, AAb+, and T1D donors. As immune cell subsets did not differ in frequency between LN draining the pancreas head, body, and tail or the SMA or MES LNs (Figure S2), we binned different LNs by anatomical origin, either pLN or mLN, for subsequent analysis. Using hierarchical clustering, we observed three different groups of disease-associated immune cell signatures, particularly in the pLN and mLN (Figure 2A). Group 1 contained pLN immune populations, including CD25+ and CD38+ T cell subsets, that decreased in frequency in AAb+ compared to ND donors and maintained a lower frequency or rebounded to normal levels in T1D. Group 2 populations increased in frequency across disease status or were elevated only in T1D. Lymphocyte subsets following this pattern included subsets of mLN CD38+ and CD25+ T cells, suggesting that CD25 and CD38 expression patterns on T cells may differ across tissue sites, depending upon disease state. Group 2 also contained pLN and mLN populations composed of cytotoxic $CD56_{dim}$CD16+ NK cells, CD27+ B cells, and several putative resident memory-like (CD69+) T cell subsets. Group 3 immune populations generally decreased in frequency in AAb+ and further in T1D donors, such as CD4+ naive T cells (Tn) cells (pLN and mLN), and CD27+ T cell subsets within the pLN. Overall, immune cell phenotypes are modulated in the pLN and mLN of AAb+ and T1D donors, with changes in AAb+ donors occurring predominantly in the pLN.

We corroborated these flow cytometry findings using an unbiased weighted gene co-expression analysis (WGCNA) approach with the CITEseq data to uncover covarying gene modules across T1D development, independent of cell identity. We only considered ND and T1D pLN in order to identify co-varying gene modules before and after overt autoimmunity. We identified seventeen gene modules covarying across the disease states, representing a diverse range of biological processes with weak correlations (Figure 2B-C, Figure S6A-B). Modules containing genes with overlapping immune function or co-correlating across clusters were of particular interest. Module 6, anchored by CD127 (*IL7R*), consisted of genes with known roles in T cell function and signaling such as *CD247*, *FYB1*[38], *CAMK4*[39], *PRKCH*[40], *ITK,* and *LEF1* (Figure 2B). This module was increased in T1D pLN CD8+ Tem/Temra and CD4 Tem/activated clusters (Figure 2C). Module 7 included genes associated with proinflammatory signaling and cytotoxic immune cells including *CCL5*, *CST7*[41], *KLRD1*, *STAT4*[42], *NKG7*, and *SRGN* (Figure 2B). Module 7 was increased in the CD8+ Tem/Temra and NK/ILC clusters (Figure 2C), suggesting more pro-inflammatory or cytotoxic gene signatures in these cell types in T1D.

Module 8 consisted of genes mainly associated with B cells (Figure 2B). This module was decreased in T1D in the IgM+ memory #2 and Naive #3 clusters, which closely overlap in phenotype with *CD69* and *CR2* expression (Figure S3), but was slightly increased in T1D in the Naive #2 cluster containing B cells with a traditional naive phenotype (Figure 2C, S3). Other modules of interest did not have a consensus function but affected all clusters within a certain cell subset. For example, module 15 was significantly decreased in T1D within most CD4+ and CD8+ T cell clusters, and markedly decreased within naive T cell subsets (Figure 2C). Module 15 was anchored by *TXK*, a gene critical for TCR signaling[43] and a regulator of interferon signaling[44], and also contained the key lymphocyte development regulator *IKZF1* (Figure 2B). Importantly, several of these highlighted modules have correlating phenotypes observed with flow cytometry (Figure 2A).

Loss and dysfunction of CD4+ Tregs in the pLN

Immune alterations before T1D onset are of particular interest to inform the development of early immune interventions capable of retaining β cell mass. In this regard, we observed a decreased frequency of CD25+ CD4+ Tem/Temra in the pLN of AAb+ donors that was maintained in the pLN of T1D donors (Figure 3A). CD4+ Tregs, phenotypically defined here by high CD25 and low CD127 surface expression, have previously been shown to be reduced in the pLN of T1D donors[35], and certain single nucleotide polymorphisms (SNPs) in or nearby the CD25-encoding gene *IL2RA* are significantly associated with T1D risk[6,45]. Indeed, the frequency of CD4+CD25+CD127low Tregs was significantly reduced in both AAb+ and T1D pLN (Figure 3B-C), suggesting that CD4+ Tregs may be altered in the pLN prior to and during T1D onset in a tissue-restricted manner, as previously reported in the NOD mouse[46]. Using CITEseq, we further explored alterations in pLN Tregs within the CD4 Tcm/Treg cluster using a set of genes associated with various Treg signatures[47,48]. Core Treg genes *FOXP3*, *IKZF4*, and *IL2RA* were significantly reduced in the CD4 Treg/Tcm cluster in both AAb+ and T1D pLN (Figure 3D), showing that this signature appears prior to T1D onset. Other genes associated with Tregs, such as *CTLA4*, were increased in AAb+ versus ND pLN while genes negatively associated with Tregs such as *IL7R* decreased in AAb+ pLN, perhaps reflecting recent activation or attempted reconstitution of Tregs in AAb+ pLN. To discern changes within Tregs specifically, we analyzed transcriptional differences between disease states within *FOXP3*+ cells in the CD4 Treg/Tcm cluster (Figure 3E). Compared to ND Tregs, AAb+ Tregs expressed lower levels of *ANTXR2*, a gene critical for extracellular matrix interactions[49], *GPR183*, a GPCR required for T cell positioning near activated T cells at the T cell zone-follicle interface[50], and several *MAML* genes associated with Notch signaling[51]. Some of these genes also had decreased expression in T1D Tregs versus ND Tregs (Figure 3E). Compared to ND pLN Tregs, Tregs in T1D pLN expressed less *FOXP1*, a gene essential for Treg stability[52], and *RUNX1*, which physically interacts with FOXP3 to upregulate Treg-associated genes[53]. To determine whether these signatures were unique to pLN Tregs, we examined the same signatures in mLN and splenic Tregs (Figure S5). We observed similar decreases in CD25+ CD4+ Tem/Temra frequency in AAb+ donors, but not T1D (Figure S5A-B). CD25+CD127low mLN CD4+ Tregs similarly decreased in mLN of AAb+ but not in T1D donors nor in spleen of any disease state (Figure S5C-D). Furthermore, we did not observe transcriptomic shifts in *FOXP3* or *IL2RA* seen in the pLN within mLN or spleen (Figure S5E). Together, these data indicate that pLN-, and to a lesser degree mLN-, specific effects on Tregs occur both in frequency and gene expression associated with Treg lineage stability and function before T1D onset.

Decreased naive T cell signatures in T1D pLN

Beyond the aforementioned changes in CD4+ Tregs, we further identified changes in the naive CD4+ T cell pool in T1D donors. Naive CD4+ T cell frequency decreased in T1D versus ND pLN (Figure 4A) and mLNs (Figure S5G), while naive CD8+ T cell frequency in the pLN did not change with disease status (Figure 4B). Additionally, the T cell biology related WGCNA module 15 (Figure 2B-C) was negatively correlated with T1D status in both naive CD4+ and CD8+ T cells in T1D (Figure 2B-C, 4C). Within the CITEseq data we identified two distinct clusters of naive CD4+ and CD8+ T cells: the first was highly enriched for naive T cell markers, termed naive #1, while the second had comparatively lower levels of naive surface markers and appeared

activated, termed naive #2 (Figure S6). Both CD4 and CD8 naive #1 clusters in the pLN displayed a stronger negative correlation of WGCNA module 15 with T1D status, compared to their respective naive #2 cluster (Figure 4C). As a percentage of total pLN CD4+ T cells, CD4 cluster naive #1 trended lower in T1D compared to ND (Figure 4D), similar to that observed by flow cytometry (Figure 4A). Conversely, cluster CD4 naive #2 trended toward an increasing proportion of cells in T1D (Figure 4D). Neither of the naive CD8+ T cell clusters changed in frequency across disease state (Figure 4B, 4E). Several genes within WGCNA module 15 have ties to T cell biology or have large expression changes across disease state (Figure 4C,F). *TXK* and *FKBP5*, a gene that coordinates with *FOXO4* to modulate cytokine production[54], were significantly decreased in T1D versus ND across all naive subsets. *IKZF1* and *ATM*, a gene critical for DNA repair during V(D)J recombination[55], were also decreased in both CD4 and CD8 naive #1 clusters but not naive #2 clusters from T1D donors. Differential gene expression analysis of all WGCNA module 15 genes within the naive T cell clusters revealed additional genes associated with phenotypic changes in naive T cells in T1D. Compared to T1D, *GYPC*, a gene involved in the cytoskeletal-plasma membrane interface, was significantly enriched in both ND pLN CD4+ and CD8+ naive #1 clusters (Figure 4F-H), and *SELL*, encoding L-selectin which facilitates homing to secondary lymphoid tissues[56], was enriched in the ND CD8 naive #2 cluster. In summary, CD4+ naive T cells decreased in frequency in the pLN in T1D donors, accompanied by decreased expression of genes involved in processes essential for naive T cell function and differentiation.

Memory CD8+ T cells display a stem-like phenotype in AAb+ and T1D pLN

CD8+ T cells play a direct role in T1D pathology due to their ability to infiltrate islets and eliminate β cells[28]. Recent work has identified stem-like pLN CD8+ T cells in NOD mice that seed terminally differentiated islet-infiltrating CD8+ T cells[34]. In human pLN, we found multiple CD8+ T cell phenotypic and transcriptomic changes before and after T1D onset. We observed a marked decrease in the proportion of cells expressing the activation markers CD25 (Figure 5A) and CD38 (Figure 5B) in AAb+ donors compared to ND. Decreased CD25 expression was noted amongst all memory CD8+ T cell subsets in AAb+ donor pLNs, and otherwise only amongst CCR7- CD8+ memory T cell populations in mLN (Figure S5I-J). The CD38+ frequency decreased in CD8+ Tn, Tn-like (Tnl), and Tcm subsets and trended lower in CD8+ Tem and Temra subsets in the pLN of AAb+ donors. In mLN and spleen, CD38 surface expression only decreased in splenic Tnl of AAb+ donors compared to ND.

We further explored T1D-associated memory CD8 Tcm/Tem/Temra CD8+ T cell alterations in relation to disease state using CITEseq (Figure 5C), focusing on the proinflammatory and cytotoxicity associated WGCNA Module 7 that positively correlated with T1D in memory CD8+ T cells (Figure 2B-C). Compared to the two other memory CD8+ T cell clusters, cells in the CD8 Tcm/Tem/Temra cluster expressed relatively higher levels of the stemness-promoting transcription factor *TCF7*. Cells in this cluster expressed molecules associated with effector and effector memory CD8+ T cells such as *EOMES*, *TOX*, *PRF1*, *GZMB*, *GZMK*, and *CXCR3*, yet lacked expression of pro-inflammatory cytokines *IFNG* and chemokine *CCL5*. Of these genes, *CXCR3*, *GZMK*, and *TOX* were differentially expressed across disease states, with expression of *CXCR3* increasing and *TOX* decreasing in AAb+ and T1D versus ND pLN (Figure 5D). *TOX* had similar expression patterns in mLN and spleen, while *CXCR3* expression decreased in T1D versus ND mLN (Figure S5M-N), suggesting that the pLN have a unique *CXCR3* gene expression pattern (Figure S5M-N). The frequency of pLN *CXCR3-TOX+GZMK+* cells recapitulated the decreased frequency of *TOX* and *GZMK* individually (Figure 5E), suggesting that these markers co-vary together. Meanwhile, *CXCR3+TOX-GZMK-* cells formed an exclusive CD8+ T cell population that trended toward increased frequency in AAb+ and T1D pLN (Figure 5E). Compared to all cells in the CD8 Tcm/Tem/Temra cluster, *CXCR3-TOX+GZMK+* cells had an activated effector phenotype, as suggested by higher surface protein levels of PD1, ICOS, CD45RO, CCR4, CCR5, CD28, and CD27 (Figure 5F). Conversely, *CXCR3+TOX-GZMK-* cells expressed lower levels of most of these surface markers and expressed increased levels of markers associated with immune suppression including CD94 and CD101 (Figure 5G). Within the CD8 Tcm/Tem/Temra cluster, *CXCR3-TOX+GZMK+* cells and *CXCR3+TOX-GZMK-* cells had opposing gene expression patterns (Figure 5H-I). Genes with higher

expression in *CXCR3-TOX+GZMK+* cells included transcription factors *IKZF2*, *BCL2*, and *MAF* (Figure 5H), while genes with higher expression in *CXCR3+TOX-GZMK-* cells included *BACH2*, a transcription factor that enforces stem-like programs[57,58], and genes associated with immunosuppression such as *KLRD1* and *CD55*. In total, pLN CD8+ T cells exhibited changes that manifested in AAb+ donors prior to T1D development: decreased cell surface expression of activation markers CD25 and CD38, a reduction of an effector *CXCR3-TOX+GZMK+* population, and an increase in a stem-like *CXCR3+TOX-GZMK-* population. The mLN and spleen also contained some of these phenotype shifts across disease states, specifically in CD25 surface expression and *TOX* expression patterns.

Cytotoxic NK cells more prominent in T1D pLN

Finally, we examined innate cell populations for potential changes associated with AAb+ or T1D status. While few overt differences were noted within most innate cell lineages present within the pLN or mLN across the different cohorts, we found that the cytotoxicity-associated WGCNA module 7 (Figure 2B-C) was positively correlated with T1D status in pLN NK cells (Figure 2A), and there was a proportional increase in the cytotoxic CD56dimCD16+ NK cell frequency in T1D pLN (Figure 6A-B). We further assessed differential gene expression within NK cell clusters between ND and T1D, focusing on genes within WGCNA module 7 and additional NK cell cytotoxicity associated genes from the KEGG pathway database[59–61]. *GZMB*, *CRTAM*, *IFNG*, and other genes associated with NK cell cytotoxicity were upregulated in T1D (Figure 6C-D). Further, the NK cell inhibitory receptor *KLRB1* was the most downregulated gene by fold change in the specific gene set (Figure 6C,E). *GZMB+* NK cells in the pLN were highly enriched in genes associated with cytotoxicity such as *NKG7*, *KLRD1*, and *GNLY* (Figure 6F), while *GZMB-* NK cells in the pLN expressed *IL1R1* and the immunosuppressive enzyme *IL4I1*[62] (Figure 6G). Compared to ND, *GZMB* expression was not increased in T1D in the mLN or spleen, while *KLRB1* decreased in expression in the mLN (Figure S5O-P), indicating that the increased cytotoxic NK cell frequency and transcriptomic signature was observed in the pLN, and not the mLN or spleen, of T1D donors.

Immune populations correlate with HLA genetic risk

HPAP collects and publicly shares extensive clinical information on each donor, allowing for the correlation of immune phenotypes with these metadata. One such parameter is HLA type, where certain alleles of HLA-DR and HLA-DQ convey significant risk for T1D[63–65]. Higher genetic risk is associated with rapid onset of T1D[66] and can distinguish between young adults with T1D versus T2D[67]. Therefore, profiling the immune system in individuals with high genetic risk may uncover immune perturbations associated with T1D disease susceptibility. Using the HLA portion of Genetic Risk Score 2 (GRS2)[68], we generated an HLA genetic risk score (HLA-GRS) that accounts for HLA DR-DQ haplotype interactions[17,68], with a higher score indicating a higher risk for disease development. As expected, T1D donors had increased HLA-GRS compared to ND (Figure 7A). We observed correlations between GRS2 and the frequency of specific pLN immune populations after controlling for the effects of disease state on immune population frequency. For example, when grouping ND and AAb+ donors, the frequency of CD8+ Tcm and Tem expressing CXCR5, HLA-DR and/or CD38 were positively correlated with HLA-GRS (Figure 7B-D). When grouping ND and T1D donors, similar populations were associated with HLA-GRS but did not reach statistical significance (data not shown), likely due to these populations being regressed out due to their increased frequency in T1D pLNs (Figure 2A). When binning AAb+ and T1D donors, the frequency of CD69+ cells in B cells and memory T cell subsets correlated positively with HLA-GRS (Figure 7E-F). The frequency of CD127+ memory T cell subsets also positively correlated with HLA-GRS, with a reciprocal decrease in the frequency of CD127- T cells (Figure 7E,G). Together, these data indicate that higher risk HLA haplotype combinations are positively associated with the frequency of certain pLN immune populations, particularly activated CD8+ memory T cells, CD127+ T cells, and CD69+ B and T cells.

Discussion

Our current knowledge of the landscape of immune perturbations during the ontogeny of T1D largely originates from the NOD mouse model and targeted analysis of specific immune subsets in human peripheral blood, with limited studies of human pLN[32,33,35]. Here, we broadly profiled lymphocyte subsets from lymphatic tissues in a large cohort of ND, AAb+, and T1D human organ donors to define immunological perturbations occurring in pLN prior to and after disease diagnosis. Compared to ND, AAb+ and T1D pLN have a reduced Treg signature and increased stem-like *CXCR3+GZMK-TOX-* CD8+ T cells. Some perturbations were T1D pLN specific, including a reduced naive T cell signature and an increased frequency of cytotoxic CD56dimCD16+ NK cells. Additionally, several immune populations in the pLN correlated with HLA-GRS independently of the effects of disease status, in particular CD8+ T cell activation signatures and increased CD69 and CD127 surface expression on T cells and/or B cells.

One of the perturbations that occurred in the pLN of AAb+ donors and persisted after T1D development was a marked decrease in CD25 expression on CD4+ and CD8+ T cells. This was most strongly reflected by an overall decrease in CD4+ Tregs, a phenomenon observed previously in T1D[35], but shown here to also manifest in AAb+ pre-T1D individuals. IL-2 signaling and production deficiencies have long been tied to T1D susceptibility, as PBMCs from children with recent onset T1D produce less IL-2[69,70], and several T1D susceptibility genomic loci are involved in IL-2 signaling[6,45]. IL-2 induced signaling responses are critical to maintaining T cell tolerance to self-antigen through the maintenance of CD4+ Tregs[71], and IL-2 signaling strongly influences CD8+ memory T cell differentiation[72]. Decreases in pLN Treg frequency in AAb+ donors highlight the evolution towards an inflammatory environment that may occur in pLN before T1D onset. Further, while CD25+ CD4+ Tem frequency in the mLN and spleen have similar patterns across disease states compared to pLN, a decline of a Treg signature in AAb+ or T1D disease states was not observed in mLN or spleen, indicating that the pLN are uniquely losing this cell population known to be critical for autoimmune control.

Loss of Tregs in AAb+ individuals was accompanied by an expansion of a stem-like CD8+ T cell population that closely resembles one that drives autoimmune diabetes in mice[34]. These stem-like CD8+ T cells were defined by expression of *TCF7* and stemness-promoting transcription factors. In human AAb+ and T1D pLN, we observed increased frequencies of less differentiated stem-like *CXCR3+GZMK-TOX-* memory CD8+ T cells expressing *BACH2*, which enforces a stem-like transcriptomic and epigenetic state[58]. Importantly, *CXCR3+* memory CD8+ cells did not change across disease state in the mLN, suggesting localization of this effect to the pLN. We further found that a *CXCR3-GZMK+TOX+* memory CD8+ T cell population defined by expression of *IKZF2*, *MAF*, and *BCL2* reciprocally decreased in the pLN of AAb+ individuals. This CD8+ T cell population shares features with *IKZF2+*KIR+ CD8+ T cells, which play a role in peripheral tolerance during inflammatory conditions[73]. It is unclear how these events are temporally associated with progression as T1D-associated AAb specificities develop[74], but a loss of Treg activity or changes in IL2 signaling could enable the survival and expansion of T1D autoantigen-specific CD8+ T cells in the local pLN environment.

We also observed expansion of cytotoxic NK cells and decreases in frequency and transcriptomic alterations in naive CD4+ and CD8+ T cells in pLN and mLN of T1D donors. As T1D progresses, β cell destruction is thought to accelerate along with proinflammatory signaling, peaking at T1D onset. Long-term inflammation drives immune aging, activation, and differentiation signatures in PBMCs of T1D donors[17]. We found that these immune activation-associated changes also occur in pLN and mLN of T1D donors. Increased surface expression of CD38, CD25, HLA-DR, and the activation-induced residency marker CD69 across many T cell subsets suggests a heightened proinflammatory environment in the pLN and mLN of T1D donors. Examining if these proinflammatory signals actively drive these phenotypes, and whether they derive from the lymph node or upstream from the pancreas, will inform therapeutic strategies for intervention during or after T1D onset.

By calculating T1D genetic risk conveyed by HLA class II alleles, we found that the frequency of memory CD8+ T cells with HLA-DR and CD38 surface expression was positively correlated with HLA-GRS, indicating that non-T1D individuals with higher-risk HLA alleles have an increased frequency of activated

memory CD8+ T cells in the pLN. While cytotoxic CD8+ T cells infiltrate islets and eliminate β cells in T1D[26,29], it is unclear how or where these autoimmune CD8+ T cells develop in humans. Evidence from the NOD mouse implicates stem-like autoimmune CD8+ T cells as a reservoir of T cells that infiltrate the pancreas[34], and we observed an expansion of stem-like memory CD8+ T cells in the pLN of AAb+ and T1D donors. It is unknown whether pLN CD8+ T cell activation observed in high-risk individuals is related to the expansion of stem-like CD8+ T cells, but a higher basal T cell activation state may potentiate expansion of autoimmune CD8+ T cells. We found that a higher HLA-GRS in AAb+ and T1D donors positively correlates with CD127 surface expression on T cells. CD127, along with the common γ chain receptor subunit, comprises the IL7R that is critical for T cell homeostatic proliferation[75], implying that pLN T cells in individuals with higher HLA-GRS may have heightened IL7 responsiveness[76]. AAb+ and T1D individuals with a higher HLA-GRS also had increased frequencies of CD69+ B and T cell subsets, indicating these individuals may have more tissue resident[77] or activated[78] immune cells. As tissue residency is critical for local tissue immune memory responses[77], further investigation is needed to explore if high risk individuals have an expanded immune memory pool that could potentiate autoimmune responses.

Our study was limited in a number of aspects. First, due to the complexities of donor acquisition, we were limited in our ability to acquire enough AAb+ organ donors with two or more T1D-associated AAbs, preventing a properly powered subanalysis of single versus multiple AAb+ donors. This limits our ability to stage the progression of immune perturbations that we observed in our cross-sectional study. Individuals without diabetes who have multiple T1D-associated AAbs are rare, and generally progress to T1D more rapidly than those with single autoantibodies[2]. Furthermore, as not all single AAb+ donors develop T1D[2,79], additional studies of pLN from donors with >1AAb+ across a range of AAb specificities will be necessary to define immunological associations with pre-T1D. Second, due to blood samples being drawn well before donor organ harvest, we determined that peripheral blood lymphocytes yielded unreliable flow cytometric and transcriptomic data (data not shown). As such, we cannot directly compare our results to previous studies focusing exclusively on peripheral blood. Third, we restricted our flow cytometric analysis to freshly isolated lymphocytes, rather than frozen lymphocytes, due to evidence of cryopreservation-induced changes in certain cell surface markers[80]. This limits subsequent flow based analysis to prospectively acquired cohorts. Fourth, we were unable to simultaneously assess B cell or T cell repertoires in the CITEseq analysis due to technical limitations from 3' mRNA transcriptomic analysis. Hence, studies of T cell or B cell T1D antigen specificity will require follow-up studies.

The deep immune profiling of rare and valuable tissue samples from organ donors collected across the spectrum of disease stages reported here provide an expansive resource for both the T1D community as well as individuals interested in lymph node immunology. This resource is structured as an immune cell atlas in an open data format with the goal of facilitating novel investigative approaches to understand disease mechanisms and identify novel targets to intervene in T1D development. Importantly, our analyses focusing on the frequencies of major immune populations by flow cytometry, or on global covariate analyses by WGCNA in the CITEseq data, did not reveal major dynamic shifts across disease states, yet found that certain subpopulations of immune cells do indeed change across disease state. The datasets provide foundational immunobiology information for the research community that could help uncover potential therapeutic targets to delay, prevent, or ameliorate T1D.

Acknowledgements
Funding: UC4-DK-112217 (to K.H.K., T.M.B., E.T.L.P., A.N., and M.R.B.), Penn IDOM Internal Pilot Grant 5-P30-DK-019525 (to M.R.B.), JDRF 3-SRA-2022-1237-S-B (to M.R.B.), JDRF PDF 3-PDF-2023-1323-A-N (to G.J.G.), Human Islet Research Network (HIRN). This manuscript used data acquired from the Human Pancreas Analysis Program (HPAP-RRID:SCR_016202), and the Human Islet Research Network (RRID:SCR_014393) consortium (UC4-DK-112217, U01-DK-123594, UC4-DK-112232, and U01-DK-123716). This research was performed with the support of the Network for Pancreatic Organ donors with Diabetes (nPOD; RRID: SCR_014641), a collaborative type 1 diabetes research project sponsored by the Juvenile Diabetes Research Foundation (JDRF) (nPOD: 5-SRA-2018-557-Q-R), and The Leona M. & Harry B. Helmsley Charitable Trust (grant 2018PG-T1D053). Genetic risk scoring data was analyzed with support from NIAID P01 to T.M.B. (AI042288). Flow cytometry data was generated in the Penn Cytomics and Cell Sorting Shared Resource Laboratory at the University of Pennsylvania (RRID: SCR_022376), which is partially supported by the Abramson Cancer Center NCI Grant (P30 016520).
Personnel: We thank K. Trihemasava, J. Shoush, and J.M.L Nordin for their assistance processing and running flow cytometry on HPAP donors, the Betts lab for their support with annotating the CITEseq dataset, and B.M.W. Golden, B.B. Golden, and B. Golden for their support.

Author Contributions
G.J.G., A.S.J, M.B.P., L.K.C., and M.R.B designed flow cytometry experiments. G.J.G., A.S.J, M.B.P., L.K.C., and J.T.H. performed flow cytometry experiments. G.J.G. analyzed the flow cytometry data. G.J.G., V. W., J.T.H., K.A., A.S.J., C.L., and J.S.G. processed HPAP tissue samples. G.J.G., V.W., and M.R.B. designed the CITEseq experiments. G.J.G performed the CITEseq experiments. G.J.G, V.W., J.T.H, M.B.P., J.J.K., E.T.L.P., and M.R.B. annotated the CITEseq dataset. G.J.G, V.W., K.A., and M.R.B. analyzed and interpreted the CITEseq dataset. M.R.S. generated the HLA-GRS. J.T.H. created tables summarizing donor information. G.J.G., V.W., and K.A. performed statistical analyses. M.A.A., K.H.K., and A.N. oversaw subject selection, clinical data acquisition, clinical data analysis, research data reporting for study subjects, and editing the manuscript. G.J.G., V.W., T.M.B, E.T.L.P., A.N., and M.R.B formulated the ideas and direction of the project. G.J.G., V.W., and M.R.B wrote the manuscript.

Declaration of Interests
The authors declare no competing interests.

Figure Legends

Figure 1. Immune profiling of pancreatic, mesenteric, and splenic lymphatic tissues
(A) UMAP representation of pLN-Tail lymphocytes and (B) splenocytes, highlighting immune lineage populations detected with flow cytometry.
(C) Hierarchical clustering of all samples within the flow cytometry dataset using major immune lineage populations. Coloring of the heatmap represents an individual sample's Z-score within the respective immune population. Immune lineage population clustering patterns were labeled and partitioned at k-means clustering level 3.
(D) PCA and (E) biplot of all flow cytometry samples using frequencies of major immune lineage populations.
(F) UMAP representation of the RNA component of the CITEseq dataset colored by tissue origin, (G) disease status, and (H) cluster annotation of each cell.
(I) Number of cells within each cluster, further subsetted by tissue type and disease state. See Figure S1-S3, Table S1-S2.

Figure 2. AAb+ and T1D associated shifts in immune phenotypes
(A) Heatmap of immune populations, detected by flow cytometry, from each tissue type that are significantly different in frequency in at least one comparison between disease states. Coloring of the heatmap represents the mean of Z-scores for a specific immune population within the specified tissue type. Statistical significance was calculated with robust one-way ANOVA, with post hoc testing using Hochberg's multiple comparison adjustment.
(B) Modules of interest generated using WGCNA analysis on scRNAseq data from pLN lymphocytes in ND and T1D disease states.
(C) Correlations of modules of interest between ND and T1D disease states, across all immune cell clusters. * is $p < 0.05$, ** is $p < 0.01$, *** is $p < 0.001$. See Figure S4.

Figure 3. Loss and dysfunction of CD4+ Tregs in the pLN
(A) Frequency of pLN CD25+ cells or (B) CD25+ CD127- CD4+ Treg cells within CD4+ T cell subsets, as determined by flow cytometry. Statistical significance determined by robust ANOVA with post hoc testing using Hochberg's multiple comparison adjustment. Boxplot represents median and interquartile range.
(C) Representative two parameter density plots of CD4+ Treg cells within the pLN, as measured by flow cytometry.
(D) Expression of CD4+ Treg-associated genes within the CD4+ Treg/Tcm cluster from pLN. Expression scaled within each gene. Statistical significance determined by Wilcoxon Rank Sum Test and p-value adjustment using the Bonferroni method.
(E) Top 20 differentially expressed genes (adjusted p value < 0.05, excluding common genes (see STAR Methods)) between disease states in *FOXP3*+ cells within the CD4 Treg/Tcm cluster in the pLN only. Statistical significance determined by Wilcoxon Rank Sum with genes with a log fold change threshold > 0.1 and p-value adjustment with the Bonferroni method across all combinatorial comparisons.
For all panels in this figure, * is $p < 0.05$, ** is $p < 0.01$, *** is $p < 0.001$. See Figure S5.

Figure 4. Decreased naive T cell signatures in T1D pLN
A) Frequency of pLN CD4+ Tn within total CD4+ T cells or (B) pLN CD8+ Tn within total CD8+ T cells, as determined by flow cytometry. Statistical significance determined by robust ANOVA with post hoc testing using Hochberg's multiple comparison adjustment. Boxplot represents median and interquartile range.
(C) Mean normalized expression of the top 10 most inter-connected genes in WGCNA module 15, plotted across the naive T cell clusters in the pLN and disease state.

(D) Frequency of the two naive CD4+ T cell clusters and (E) the two naive CD8+ T cell clusters in the pLN, across disease states. Boxplot represents median and interquartile range. P value determined by Wilcoxon ranked sum test with Benjamini-Hochberg multiple test correction.
(F) Normalized expression of genes of interest from WGCNA module 15, from the pLN only. Statistical significance determined by Wilcoxon Rank Sum Test with a log fold change threshold of 0.1 and p-value adjustment using the Bonferroni method.
(G) Differentially expressed WGCNA module 15 genes CD4 Naive #1 and CD4 Naive #2 clusters and (H) CD8 Naive #1 and CD8 Naive #2 clusters from the pLN, between ND and T1D donors. Statistical significance tested using Wilcoxon Rank Sum Test with p-value adjustment using the Bonferroni method.
For all panels in this figure, * is $p < 0.05$, ** is $p < 0.01$, *** is $p < 0.001$. See Figure S5-S6.

Figure 5. Memory CD8+ T cells display a stem-like phenotype in AAb+ and T1D pLN
(A) Frequency of pLN CD25+ cells or (B) CD38+ cells within pLN CD8+ T cell subsets, as determined by flow cytometry. Statistical significance determined by robust ANOVA with post hoc testing using Hochberg's multiple comparison adjustment. Boxplot represents median and interquartile range.
(C) WGCNA module 7 and effector CD8+ T cell genes of interest mean normalized expression in the pLN, across disease state.
(D) Normalized expression of *CXCR3*, *GZMK*, and *TOX* in CD8 Tcm/Tem/Temra cells in the pLN. Statistical significance determined by Wilcoxon Rank Sum test with Bonferroni correction done between all combinatorial tests. Dashed red line indicates the exclusive threshold (> 0.5) for demarcating positive gene expression for later plots.
(E) Frequency of pLN CD8 Tcm/Tem/Temra cells expressing permutations of *CXCR3*, *GZMK*, and *TOX*, across disease state. P value determined by Wilcoxon rank sum test with Benjamini-Hochberg multiple test correction. (F) Differential surface protein ADTs enriched in *CXCR3-TOX+GZMK+* cells and (G) *CXCR3+TOX-GZMK-* cells compared to all other permutations of *CXCR3*, *GZMK*, and *TOX* expression within CD8 Tcm/Tem/Temra cluster in the pLN. Total CD8+ T cells, total CD8+ T cells, the NK/ILC cell cluster, total B cells, and total monocytes were used as comparators. Statistical significance determined by Wilcoxon rank sum test on ADTs with log fold change threshold > 0.1 followed by Bonferroni multiple test adjustment (adjusted p value < 0.05 denotes significant differential expression). Populations of interest highlighted by the black outline.
(H) Genes differentially expressed in *CXCR3-TOX+GZMK+* cells and (I) *CXCR3+TOX-GZMK-* cells compared to all other permutations of *CXCR3*, *GZMK*, and *TOX* expression within CD8 Tcm/Tem/Temra cluster in the pLN. Statistical significance determined by Wilcoxon rank sum test with log fold change threshold > 0.25 followed by Bonferroni multiple test adjustment (adjusted p value < 0.05). Populations of interest highlighted by the black outline.
For all panels in this figure, * is $p < 0.05$, ** is $p < 0.01$, *** is $p < 0.001$. See Figure S5.

Figure 6. Cytotoxic NK cells more prominent in T1D pLN
(A) Frequency of CD56dimCD16+ NK cells within the pLN, as measured by flow cytometry. Statistical significance determined by robust ANOVA with post hoc testing using Hochberg's multiple comparison adjustment. Boxplot represents median and interquartile range.
(B) Representative two parameter density plots images of NK cell subsets within the pLN.
(C) List of differentially expressed genes, ranked by descending log2 fold change, of genes that are significantly more expressed in T1D pLN. Cells are from a combination of the NK and NK/ILC clusters, from the pLN only. Gene sets to test came from the Module 7 of the WGCNA analysis, which was significantly increased in NK cell clusters in T1D, and from the "Natural killer cell mediated cytotoxicity" gene set from Kyoto Encyclopedia of Genes and Genomes (KEGG).

(D) Normalized expression of *GZMB* and (E) *KLRB1* within the combined NK and NK/ILC clusters in the pLN. Statistical significance tested using Wilcoxon Rank Sum Test with p-value adjustment using the Bonferroni method.
(F) Mean normalized expression of genes significantly increased in *GZMB*+ and (G) *GZMB*- cells from the combined NK and NK/ILC clusters in the pLN. P value determined by Wilcoxon Rank Sum Test with p-value adjustment using the Bonferroni method.
For all panels in this figure, * is $p < 0.05$, ** is $p < 0.01$, *** is $p < 0.001$. See Figure S5.

Figure 7. Immune populations correlate with HLA genetic risk
(A) HLA-GRS score of donors in the cohort. Boxplot represents median and interquartile range. P value generated with Dunn's test with multiple hypothesis correction adjustment using Holm's method. * is $p < 0.05$.
(B) Immune populations that significantly correlate with HLA-GRS in ND and AAb+ donors. Grey line represents an adjusted p value ≥ 0.05. Dot fill represents a Kendall tau correlation value corrected for disease state effects.
(C) and (D) Representative plots of HLA-GRS versus immune population frequency in ND and AAb+ donors. τ_c is the Kendall tau correlation value corrected for disease state effects, represented by the blue linear regression line with standard error in grey. p_c is the p value adjusted for disease state effects and corrected with Benjamini-Hochberg multiplicity adjustment.
(E) Immune populations that significantly correlate with HLA-GRS in AAb+ and T1D donors. All plot parameters follow (B).
(F) and (G) Representative plots of HLA-GRS versus immune population frequency in AAb+ and T1D donors. All plot parameters follow (C) and (D).

Methods

RESOURCE AVAILABILITY

Lead Contact

Further information and requests for resources and reagents should be directed to and will be fulfilled by the lead contact, Michael R. Betts (betts@pennmedicine.upenn.edu).

Materials Availability

There are restrictions on the availability of donor tissue samples, due to some tissue samples being depleted from these studies and due to the need for a material transfer agreement. This study did not generate new unique reagents.

Data and Code Availability

All de-identified human flow cytometry, sequencing based, clinical data have been deposited on PANC-DB (https://hpap.pmacs.upenn.edu/). Raw sequencing based data are also deposited in Genbank under accession number GSE221787. All original code has been deposited at GitHub at https://github.com/betts-lab/hpap-tissue-citeseq. Exceptions are the code used to generate HLA-GRS, which can be found at https://github.com/sethsh7/hla-prs-toolkit version 0.22a[68], and code for ADT and HTO preprocessing, which is found at https://github.com/betts-lab/scc-proc. All data and code are publicly available as of the date of publication. DOIs and Accession numbers are listed in the key resources table. Any additional information required to reanalyze the data reported in this paper is available from the lead contact upon request.

EXPERIMENTAL MODEL AND STUDY PARTICIPANTS

Experimental model and study participant methods are described[29,81]. Details on the samples obtained through the HPAP are available online at https://hpap.pmacs.upenn.edu and described[37]. Whole organ samples are obtained via the local organ procurement organization or via University of Florida/nPOD. The consent for procurement of research pancreata was obtained by staff of the organ procurement organization. All human samples were de-identified and IRB exempt. Donors were evaluated for autoantibody status (GAD, IA-2, IAA and ZnT8), C-peptide levels, and underwent clinical chart review. Clinical data including diagnosis of T1D, HbA1c, BMI, age, gender, HLA type, and more are recorded in the HPAP database. Additional data from histology, immunophenotyping, repertoire profiling, metabolic and transcriptomic studies are generated on all HPAP donors, providing a shared and publicly available comprehensive resource.

METHOD DETAILS

Tissues and cells

To isolate pancreatic and mesenteric LN lymphocytes, LNs obtained from organ donors were submerged in 5 mL R10 media (RPMI + 10% FBS + 1% penicillin/streptomycin + 2mM L-glutamine) supplemented with 10U/mL DNase I (Roche), cleaned of visceral fat, and cut into small pieces (~2mm x ~2mm). Tissue fragments were placed into a sterile 70 µm mesh (Miltenyi Biotech) and pushed through the mesh with the blunt end of a sterile 5 mL syringe plunger. Residual tissues and cells in the mesh were washed with 45 mL of R10 + DNAse, centrifuged at 500 xg for 7 minutes, resuspended in 10 mL of R10 + DNAse, and counted. To isolate splenocytes, approximately 30 g of spleen tissue was placed in R10 supplemented with 10U/mL DNase I and 3 mg/ml collagenase D (Sigma), the capsule was removed, and remaining tissue was cut into 4mm x 4mm pieces. The tissue was then mechanically dissociated using a GentleMACS (Miltenyi Biotech) and incubated at 37 C for 15 min with gentle inversion. After digestion, the cell suspension was filtered through a 100 µm strainer, and erythrocytes were lysed by ACK buffer (Corning). Post-ACK, cells were resuspended in R10 media and filtered through a sterile 70 µm mesh. Splenic mononuclear cells were isolated by density gradient

centrifugation using Ficoll-Paque. Viable cell suspensions from LN and spleen were cryopreserved in FBS + 10% DMSO and stored at -150°C until thawing.

Flow cytometry acquisition and analysis

All antibody staining was done on freshly isolated cells following a protocol detailed elsewhere[82]. After washing with phosphate-buffered saline (PBS), cells (whole blood derived leukocytes or isolated lymphocytes) were prestained for the chemokine receptor CCR7 for 15 min at 37°C 5% CO_2. All following incubations were performed at room temperature. Cells were stained for viability exclusion using Live/Dead Fixable Aqua (Invitrogen) for 10 minutes, followed by a 20 minute incubation with a panel of directly conjugated antibodies and Trustain (BioLegend) diluted with fluorescence-activated cell sorting (FACS) buffer (PBS containing 0.1% sodium azide and 1% bovine serum albumin) and Brilliant Stain Buffer (BD Biosciences). The cells were washed in FACS buffer and fixed in PBS containing 4% paraformaldehyde (Electron Microscopy Sciences). Cells were stored at 4°C in the dark until acquisition. All flow cytometry data was collected on a BD FACSymphony A5 cytometer (BD Biosciences). FlowJo software version 10.9 was used to generate population frequencies and representative flow cytometry plots. R was used for further analysis of these exported population frequencies.

CITEseq sample processing and library generation

Eight samples were run simultaneously for each round of CITEseq, balancing both tissue type and disease state across runs. Cryopreserved cells were thawed by gentle shaking in a 37°C water bath until the cell suspension was partially thawed, which was immediately decanted into cold R10 medium + DNAse. Thawed cells were centrifuged at 500 xg for 7 minutes, then resuspended in room temperature R10 + DNAse. Cells were rested in R10 + DNAse at 2 x10^6 cells/mL for 2 hr at 37°C with 5% CO_2. All following cell preparation and antibody staining steps, including centrifugation, were done at 4°C. After resting, cells were centrifuged at 500 xg for 7 minutes and resuspended in 1 mL ice cold Cell Stain Buffer (CSB, BioLegend). Samples were filtered through a sterile pre-wet 70 µm mesh, followed by a 2 mL wash with CSB. 500k live cells that passed through the mesh were spun at 200 xg for 10 minutes and resuspended in CSB. Trustain was added to each sample at a 1:10 dilution and incubated on ice for 10 minutes. After, each sample received a unique hashing antibody (BioLegend) following manufacturer's instructions. Totalseq-A antibody cocktail (BioLegend), reconstituted in CSB following the manufacturer's protocol, was added to each sample at the manufacturer's recommended concentration. After a 30 minute incubation on ice, cells were washed 3X with ice cold CSB, counted, and pooled in CSB at 2000 cells/µL with ~125K cells from each sample. The pooled sample was filtered through a 40µm FlowMi strainer (Sigma) and counted. Pooled samples were run at 17.5k cells/well on a Chromium X (10X Genomics) using the Chromium Next GEM Single Cell 3' HT or RT kit v3.1 (10X Genomics). Single cell sequencing library preparations for the RNA modality followed the manufacturer's protocol, with the exception of spiking in primers at step 2.2 that amplify ADT and HTO sequences. 1 µL of 0.2 µM ADT additive primer (sequence: CCTTGGCACCCGAGAATT*C*C) and 1 µL of 0.1 uM HTO additive primer (sequence: GTGACTGGAGTTCAGACGTGTGCTCTTCCGAT*C*T) was spiked into each individual sample prep. Preparation of the ADT and HTO single cell sequencing libraries followed manufacturer's protocol (BioLegend) and described elsewhere (cite-seq.com)[83,84]. Briefly, at step 2.3d, 60 µL of supernatant was collected, 140 µL of SPRIselect reagent (Beckman Coulter) was added to the collected supernatant, washed twice with 80% ethanol, and eluted with 90 µL EB (Qiagen). For the respective ADT and HTO modalities, antibody-derived oligomers were amplified and indexed by mixing 45 µL eluent with 50 µL of KAPA HiFi HotStart ReadyMix (KAPA Biosystems) and 5 µL of forward/reverse indexing primers (Biolegend). Amplification settings for the ADT modality were as follows: 95 °C 3 min, ~8 cycles of 95 °C 20 sec, 60 °C 30 sec, and 72 °C 20 sec, followed by 72 °C for 5 min and ending with hold at 4 °C. Amplification settings for the HTO modality were the same except for a 64 °C annealing temperature. Post-amplification, ADT and HTO libraries were purified with a 1.2X SPRIselect cleanup and eluted with 30 µL EB. All final libraries were quantified using a Qubit dsDNA HS Assay kit (Invitrogen) and a High Sensitivity D1000 DNA tape (Agilent) on a Tapestation D4200 (Agilent).

CITEseq library sequencing
Sequencing runs were performed on the NovaSeq 6000 platforms (Illumina) with a target of at least 10,000 reads per cell for ADT libraries, 25,000 reads per cell for RNA libraries, and 500 reads per cell for HTO libraries.

CITEseq preprocessing
The cellranger (7.0.0; 10X Genomics) suite of tools were used for all preprocessing steps for the RNA component. Raw BCL files were demultiplexed using the cellranger mkfastq tool, resulting in fastq files for each lane used in the 10X Genomics chip. Fastq files were processed into cell by gene matrices using the cellranger count tool by aligning against the hg38 reference genome. The resultant matrices were used for downstream analyses. For ADT and HTO, raw BCL files were demultiplexed using bcl2fastq2 (Illumina) to create fastq files that correspond to each lane used in the 10X Genomics chip. Fastq files were then counted using a variation of the kite pipeline (https://github.com/pachterlab/kite) which uses kallisto and bustools[85] for alignment, barcode correction, and counting to create cell by feature matrices. Code for ADT and HTO preprocessing is found here: https://github.com/betts-lab/scc-proc.

CITEseq modality processing and dehashing
The RNA filtered feature barcode matrix (as outputted from cellranger count) was loaded into R (v4.1.1) and Seurat (v4.1.1) to create a Seurat object after filtering out for wells that had low cell recovery and/or poor quality control metrics as determined by cellranger. Cells were then further filtered by the following criteria for initial quality checking: number of features > 200 & number of features < 6000 & percentage of mitochondrial reads < 12.5%. RNA counts were then normalized on a per cell basis. The ADT barcode matrix (as outputted from kallisto bustools) was loaded into the emptyDrops function (DropletUtils v1.14.2) with a minimum threshold of 100 UMI counts to determine what barcodes are associated with empty droplets (false discovery rate < 0.01). The empty droplets were filtered out of the ADT matrix. The intersection of usable barcodes was determined between the QC filtered RNA modality, the QC filtered ADT modality, and the HTO barcode matrix. The Seurat object was filtered to retain only barcodes that were detected/passing QC in all three modalities. After adding the ADT and HTO modalities as separate Assay objects, we normalized the HTO data within each hashtag. The HTODemux() function in Seurat with the argument (positive.quantile = 0.99) was used to demultiplex samples based on hashtag. Samples that were classified as singlets were kept for downstream analyses.

Modality integration and clustering: All runs were merged into a single Seurat object. ADT data were scaled and normalized using the centered-log ratio method by cell. Principal component analysis was performed for RNA and ADT separately and resultant principal components were each used as input for batch effect correction using Harmony[86] with grouping variables set by donor and by each chip used for droplet emulsions. The batch effect corrected RNA-based principal components were used to generate a shared nearest neighbor (sNN) graph. Using the sNN graph, clustering was performed with the Leiden algorithm and the following settings for the FindClusters method in Seurat (method = “igraph” and resolution = 1). An uniform manifold approximation and projection (UMAP) representation of the data was constructed from the sNN graph for visualization purposes. Using both the ADT and RNA modalities, clusters were manually annotated. Clusters with multiplet signatures or phenotypes indicative of poor sample quality/viability were discarded. Given the known viability difficulties with human biopsy samples, we used a heat shock protein (HSP) gene set list (Group 582) from the HUGO Gene Nomenclature Committee (HGNC)[87]. These genes were fed into the AddModuleScore function in Seurat to generate a heat shock module. To remove confounding effects associated with heat shock response, cells with a score less than the 95th percentile of overall heat shock module scores were kept for downstream analysis.

Weighted gene co-expression network analysis (WGCNA) for pancreatic lymph node samples

The dataset after clustering and quality control filtering were filtered for cells from the pancreatic lymph nodes and from donors associated with ND or T1D disease status for a more targeted analysis without confounding effects from other tissue sites and the inherent diversity of donors labeled as autoantibody positive. A WGCNA was constructed using the WGCNA[88] and hdWGCNA[89] packages where metacells were formed based on the following grouping variables: donor, disease status, and condensed phenotype from manual annotations. The resulting topological co-expression network was used to identify modules and assess correlations with disease status and manual phenotypes. All specific function parameters and steps for WGCNA are detailed in the study GitHub repository (see Resource Availability).

HLA-GRS calculation and correlation to immune populations

Phasing of HLA-DQA1 and HLA-DQB1 genotypes was inferred via comparison with published haplotype frequencies from European Americans[90]. HLA-DQA1-DQB1 haplotypes were used to calculate the HLA component of the T1D polygenic risk score, GRS2, according to methods developed by Sharp, et al[68]. Scoring considered additive odds ratios for 14 individual haplotypes and interactions for 18 non-additive haplotype combinations as in the Polygenic Risk Score (PRS) Toolkit for HLA (v0.22a)[68]. Correlations between HLA-GRS and immune population frequency were computed using partial correlation analysis from the ppcor package.

Graphics

All figures were made in R with the following packages: grid, ggplot2[91], ComplexHeatmap, Seurat, hdWGCNA, and patchwork. All code to produce figures can be found in the study GitHub repository (see Resource Availability). Annotations were added to the R-generated figures using Adobe Illustrator (v.22.2.3).

QUANTIFICATION AND STATISTICAL ANALYSES

For flow cytometry, all statistical analyses were run in R with the rstatix, ggpubr, and multicomp packages. Non-parametric analyses between two groups were performed with a two sample Wilcoxon test, with multiple hypothesis correction using Holm's method when appropriate, using the rstatix package. Non-parametric analyses between 3 or more groups was performed with Dunn's test, with Holm's method for multiple hypothesis correction adjustment, using the rstatix package. Parametric comparisons between 3 or more groups were performed with robust one-way ANOVA in the WRS2 package, with post hoc testing using Hochberg's multiple comparison adjustment and tr = 0.1. If cold ischemia was found to affect the frequency of an immune population, ANCOVA was used to control for the effect of cold ischemia on immune population frequency while comparing 3 or more groups, with post hoc analysis performed with Tukey's test, using the multicomp package. Each dot in a plot depicting summarized flow cytometry data is an individual sample. Sample distributions represented by a boxplot, with the median depicted as the center value, quartile ranges forming the box edges, and whiskers depicting the minimum to maximum distribution. Correlations between HLA-GRS and immune population frequency were run using the partial Kendall rank correlation while controlling for the confounding variables of disease state and cold ischemia time. Correlation p-values were adjusted for multiple comparisons using Benjamini-Hochberg multiple test correction. For CITEseq analysis, samples were quality controlled as explained in the "CITEseq modality processing and dehashing" section. To help elucidate more specific cell type differences in differential gene analysis, a common set of differentially expressed genes was computed for each manually annotated cluster between disease states using the Wilcoxon Rank Sum implementation in Seurat FindAllMarkers with a log fold change threshold of 0.1. Any differential genes that were found in more than 12 clusters were labeled as common genes that were largely independent of cell phenotype. Combinatorial differential expression testing was performed with Seurat FindMarkers (Wilcoxon Rank Sum) followed by Bonferroni correction for multiple tests calculated across all tests performed across the combinations. Unless otherwise stated in text or figure legends, significance by

statistical test was set as adjusted p value < 0.05. * is p < 0.05, ** is p < 0.01, *** is p < 0.001 for all figures. Refer to figure legends for the application and details of each test.

ADDITIONAL RESOURCES

All de-identified human flow cytometry, sequencing based, clinical data have been deposited on PANC-DB (https://hpap.pmacs.upenn.edu/). Additional data from histology, immunophenotyping, repertoire profiling, metabolic and transcriptomic studies are generated on all HPAP donors, providing a shared and publicly available comprehensive resource.

References

1. Atkinson, M. A., Eisenbarth, G. S. & Michels, A. W. Type 1 diabetes. *Lancet* **383,** 69–82 (2014).
2. Insel, R. A., Dunne, J. L., Atkinson, M. A., Chiang, J. L., Dabelea, D., Gottlieb, P. A., Greenbaum, C. J., Herold, K. C., Krischer, J. P., Lernmark, Å., Ratner, R. E., Rewers, M. J., Schatz, D. A., Skyler, J. S., Sosenko, J. M. & Ziegler, A.-G. Staging presymptomatic type 1 diabetes: a scientific statement of JDRF, the Endocrine Society, and the American Diabetes Association. *Diabetes Care* **38,** 1964–1974 (2015).
3. Oram, R. A., McDonald, T. J., Shields, B. M., Hudson, M. M., Shepherd, M. H., Hammersley, S., Pearson, E. R., Hattersley, A. T. & UNITED Team. Most people with long-duration type 1 diabetes in a large population-based study are insulin microsecretors. *Diabetes Care* **38,** 323–328 (2015).
4. Williams, G. M., Long, A. E., Wilson, I. V., Aitken, R. J., Wyatt, R. C., McDonald, T. J., Wong, F. S., Hattersley, A. T., Williams, A. J. K., Bingley, P. J. & Gillespie, K. M. Beta cell function and ongoing autoimmunity in long-standing, childhood onset type 1 diabetes. *Diabetologia* **59,** 2722–2726 (2016).
5. Gubitosi-Klug, R. A., Braffett, B. H., Hitt, S., Arends, V., Uschner, D., Jones, K., Diminick, L., Karger, A. B., Paterson, A. D., Roshandel, D., Marcovina, S., Lachin, J. M., Steffes, M., Palmer, J. P. & DCCT/EDIC Research Group. Residual β cell function in long-term type 1 diabetes associates with reduced incidence of hypoglycemia. *J. Clin. Invest.* **131,** (2021).
6. Todd, J. A., Walker, N. M., Cooper, J. D., Smyth, D. J., Downes, K., Plagnol, V., Bailey, R., Nejentsev, S., Field, S. F., Payne, F., Lowe, C. E., Szeszko, J. S., Hafler, J. P., Zeitels, L., Yang, J. H. M., Vella, A., Nutland, S., Stevens, H. E., Schuilenburg, H., Coleman, G., Maisuria, M., Meadows, W., Smink, L. J., Healy, B., Burren, O. S., Lam, A. A. C., Ovington, N. R., Allen, J., Adlem, E., Leung, H.-T., Wallace, C., Howson, J. M. M., Guja, C., Ionescu-Tîrgovişte, C., Genetics of Type 1 Diabetes in Finland, Simmonds, M. J., Heward, J. M., Gough, S. C. L., Wellcome Trust Case Control Consortium, Dunger, D. B., Wicker, L. S. & Clayton, D. G. Robust associations of four new chromosome regions from genome-wide analyses of type 1 diabetes. *Nat. Genet.* **39,** 857–864 (2007).
7. Nejentsev, S., Howson, J. M. M., Walker, N. M., Szeszko, J., Field, S. F., Stevens, H. E., Reynolds, P., Hardy, M., King, E., Masters, J., Hulme, J., Maier, L. M., Smyth, D., Bailey, R., Cooper, J. D., Ribas, G., Campbell, R. D., Clayton, D. G., Todd, J. A. & Wellcome Trust Case Control Consortium. Localization of type 1 diabetes susceptibility to the MHC class I genes HLA-B and HLA-A. *Nature* **450,** 887–892 (2007).
8. Shapiro, M. R., Thirawatananond, P., Peters, L., Sharp, R. C., Ogundare, S., Posgai, A. L., Perry, D. J. & Brusko, T. M. De-coding genetic risk variants in type 1 diabetes. *Immunol. Cell Biol.* **99,** 496–508 (2021).
9. Sims, E. K., Bundy, B. N., Stier, K., Serti, E., Lim, N., Long, S. A., Geyer, S. M., Moran, A., Greenbaum, C. J., Evans-Molina, C., Herold, K. C. & Type 1 Diabetes TrialNet Study Group. Teplizumab improves and stabilizes beta cell function in antibody-positive high-risk individuals. *Sci. Transl. Med.* **13,** (2021).
10. Long, S. A., Thorpe, J., DeBerg, H. A., Gersuk, V., Eddy, J. A., Harris, K. M., Ehlers, M., Herold, K. C., Nepom, G. T. & Linsley, P. S. Partial exhaustion of CD8 T cells and clinical response to teplizumab in new-onset type 1 diabetes. *Science Immunology* **1,** eaai7793 (2016).
11. Kenefeck, R., Wang, C. J., Kapadi, T., Wardzinski, L., Attridge, K., Clough, L. E., Heuts, F., Kogimtzis, A., Patel, S., Rosenthal, M., Ono, M., Sansom, D. M., Narendran, P. & Walker, L. S. K. Follicular helper T cell signature in type 1 diabetes. *J. Clin. Invest.* **125,** 292–303 (2015).

12. Abdelsamed, H. A., Zebley, C. C., Nguyen, H., Rutishauser, R. L., Fan, Y., Ghoneim, H. E., Crawford, J. C., Alfei, F., Alli, S., Ribeiro, S. P., Castellaw, A. H., McGargill, M. A., Jin, H., Boi, S. K., Speake, C., Serti, E., Turka, L. A., Busch, M. E., Stone, M., Deeks, S. G., Sekaly, R.-P., Zehn, D., James, E. A., Nepom, G. T. & Youngblood, B. Beta cell-specific CD8+ T cells maintain stem cell memory-associated epigenetic programs during type 1 diabetes. *Nat. Immunol.* **21,** 578–587 (2020).
13. Pesenacker, A. M., Chen, V., Gillies, J., Speake, C., Marwaha, A. K., Sun, A., Chow, S., Tan, R., Elliott, T., Dutz, J. P., Tebbutt, S. J. & Levings, M. K. Treg gene signatures predict and measure type 1 diabetes trajectory. *JCI Insight* **4,** (2019).
14. Hanley, P., Sutter, J. A., Goodman, N. G., Du, Y., Sekiguchi, D. R., Meng, W., Rickels, M. R., Naji, A. & Luning Prak, E. T. Circulating B cells in type 1 diabetics exhibit fewer maturation-associated phenotypes. *Clin. Immunol.* **183,** 336–343 (2017).
15. Stensland, Z. C., Magera, C. A., Broncucia, H., Gomez, B. D., Rios-Guzman, N. M., Wells, K. L., Nicholas, C. A., Rihanek, M., Hunter, M. J., Toole, K. P., Gottlieb, P. A. & Smith, M. J. Identification of an anergic BND cell-derived activated B cell population (BND2) in young-onset type 1 diabetes patients. *J. Exp. Med.* **220,** (2023).
16. Xhonneux, L.-P., Knight, O., Lernmark, Å., Bonifacio, E., Hagopian, W. A., Rewers, M. J., She, J.-X., Toppari, J., Parikh, H., Smith, K. G. C., Ziegler, A.-G., Akolkar, B., Krischer, J. P. & McKinney, E. F. Transcriptional networks in at-risk individuals identify signatures of type 1 diabetes progression. *Sci. Transl. Med.* **13,** (2021).
17. Shapiro, M. R., Dong, X., Perry, D. J., McNichols, J. M., Thirawatananond, P., Posgai, A. L., Peters, L. D., Motwani, K., Musca, R. S., Muir, A., Concannon, P., Jacobsen, L. M., Mathews, C. E., Wasserfall, C. H., Haller, M. J., Schatz, D. A., Atkinson, M. A., Brusko, M. A., Bacher, R. & Brusko, T. M. Human immune phenotyping reveals accelerated aging in type 1 diabetes. *JCI Insight* **8,** (2023).
18. Poon, M. M. L., Caron, D. P., Wang, Z., Wells, S. B., Chen, D., Meng, W., Szabo, P. A., Lam, N., Kubota, M., Matsumoto, R., Rahman, A., Luning Prak, E. T., Shen, Y., Sims, P. A. & Farber, D. L. Tissue adaptation and clonal segregation of human memory T cells in barrier sites. *Nat. Immunol.* **24,** 309–319 (2023).
19. Buggert, M., Vella, L. A., Nguyen, S., Wu, V. H., Chen, Z., Sekine, T., Perez-Potti, A., Maldini, C. R., Manne, S., Darko, S., Ransier, A., Kuri-Cervantes, L., Japp, A. S., Brody, I. B., Ivarsson, M. A., Gorin, J.-B., Rivera-Ballesteros, O., Hertwig, L., Antel, J. P., Johnson, M. E., Okoye, A., Picker, L., Vahedi, G., Sparrelid, E., Llewellyn-Lacey, S., Gostick, E., Sandberg, J. K., Björkström, N., Bar-Or, A., Dori, Y., Naji, A., Canaday, D. H., Laufer, T. M., Wells, A. D., Price, D. A., Frank, I., Douek, D. C., Wherry, E. J., Itkin, M. G. & Betts, M. R. The Identity of Human Tissue-Emigrant CD8+ T Cells. *Cell* **183,** 1946–1961.e15 (2020).
20. Buggert, M., Price, D. A., Mackay, L. K. & Betts, M. R. Human circulating and tissue-resident memory CD8+ T cells. *Nat. Immunol.* **24,** 1076–1086 (2023).
21. Akkaya, M., Kwak, K. & Pierce, S. K. B cell memory: building two walls of protection against pathogens. *Nat. Rev. Immunol.* **20,** 229–238 (2020).
22. Hashemi, E. & Malarkannan, S. Tissue-Resident NK Cells: Development, Maturation, and Clinical Relevance. *Cancers* **12,** (2020).
23. Babon, J. A. B., DeNicola, M. E., Blodgett, D. M., Crèvecoeur, I., Buttrick, T. S., Maehr, R., Bottino, R., Naji, A., Kaddis, J., Elyaman, W., James, E. A., Haliyur, R., Brissova, M., Overbergh, L., Mathieu, C., Delong, T., Haskins, K., Pugliese, A., Campbell-Thompson, M., Mathews, C., Atkinson, M. A., Powers, A. C., Harlan, D. M. & Kent, S. C. Analysis of self-antigen specificity of islet-infiltrating T cells from human donors with type 1 diabetes. *Nat. Med.* **22,** 1482–1487 (2016).
24. Culina, S., Lalanne, A. I., Afonso, G., Cerosaletti, K., Pinto, S., Sebastiani, G., Kuranda, K., Nigi, L., Eugster, A., Østerbye, T., Maugein, A., McLaren, J. E., Ladell, K., Larger, E., Beressi, J.-P., Lissina, A., Appay, V., Davidson, H. W., Buus, S., Price, D. A., Kuhn, M., Bonifacio, E., Battaglia, M., Caillat-Zucman, S., Dotta, F., Scharfmann, R., Kyewski, B., Mallone, R. & ImMaDiab Study Group. Islet-reactive CD8 + T cell frequencies in the pancreas, but not in blood, distinguish type 1 diabetic patients from healthy donors.

Science Immunology **3,** (2018).
25. Opie, E. L. ON THE RELATION OF CHRONIC INTERSTITIAL PANCREATITIS TO THE ISLANDS OF LANGERHANS AND TO DIABETES MELUTUS. *J. Exp. Med.* **5,** 397–428 (1901).
26. Coppieters, K. T., Dotta, F., Amirian, N., Campbell, P. D., Kay, T. W. H., Atkinson, M. A., Roep, B. O. & von Herrath, M. G. Demonstration of islet-autoreactive CD8 T cells in insulitic lesions from recent onset and long-term type 1 diabetes patients. *J. Exp. Med.* **209,** 51–60 (2012).
27. Leete, P., Willcox, A., Krogvold, L., Dahl-Jørgensen, K., Foulis, A. K., Richardson, S. J. & Morgan, N. G. Differential Insulitic Profiles Determine the Extent of β-Cell Destruction and the Age at Onset of Type 1 Diabetes. *Diabetes* **65,** 1362–1369 (2016).
28. Campbell-Thompson, M., Fu, A., Kaddis, J. S., Wasserfall, C., Schatz, D. A., Pugliese, A. & Atkinson, M. A. Insulitis and β-Cell Mass in the Natural History of Type 1 Diabetes. *Diabetes* **65,** 719–731 (2016).
29. Wang, Y. J., Traum, D., Schug, J., Gao, L., Liu, C., HPAP Consortium, Atkinson, M. A., Powers, A. C., Feldman, M. D., Naji, A., Chang, K.-M. & Kaestner, K. H. Multiplexed In Situ Imaging Mass Cytometry Analysis of the Human Endocrine Pancreas and Immune System in Type 1 Diabetes. *Cell Metab.* **29,** 769–783.e4 (2019).
30. Damond, N., Engler, S., Zanotelli, V. R. T., Schapiro, D., Wasserfall, C. H., Kusmartseva, I., Nick, H. S., Thorel, F., Herrera, P. L., Atkinson, M. A. & Bodenmiller, B. A Map of Human Type 1 Diabetes Progression by Imaging Mass Cytometry. *Cell Metab.* **29,** 755–768.e5 (2019).
31. Gagnerault, M.-C., Luan, J. J., Lotton, C. & Lepault, F. Pancreatic lymph nodes are required for priming of beta cell reactive T cells in NOD mice. *J. Exp. Med.* **196,** 369–377 (2002).
32. Kent, S. C., Chen, Y., Bregoli, L., Clemmings, S. M., Kenyon, N. S., Ricordi, C., Hering, B. J. & Hafler, D. A. Expanded T cells from pancreatic lymph nodes of type 1 diabetic subjects recognize an insulin epitope. *Nature* **435,** 224–228 (2005).
33. Seay, H. R., Yusko, E., Rothweiler, S. J., Zhang, L., Posgai, A. L., Campbell-Thompson, M., Vignali, M., Emerson, R. O., Kaddis, J. S., Ko, D., Nakayama, M., Smith, M. J., Cambier, J. C., Pugliese, A., Atkinson, M. A., Robins, H. S. & Brusko, T. M. Tissue distribution and clonal diversity of the T and B cell repertoire in type 1 diabetes. *JCI Insight* **1,** e88242 (2016).
34. Gearty, S. V., Dündar, F., Zumbo, P., Espinosa-Carrasco, G., Shakiba, M., Sanchez-Rivera, F. J., Socci, N. D., Trivedi, P., Lowe, S. W., Lauer, P., Mohibullah, N., Viale, A., DiLorenzo, T. P., Betel, D. & Schietinger, A. An autoimmune stem-like CD8 T cell population drives type 1 diabetes. *Nature* **602,** 156–161 (2022).
35. Ferraro, A., Socci, C., Stabilini, A., Valle, A., Monti, P., Piemonti, L., Nano, R., Olek, S., Maffi, P., Scavini, M., Secchi, A., Staudacher, C., Bonifacio, E. & Battaglia, M. Expansion of Th17 cells and functional defects in T regulatory cells are key features of the pancreatic lymph nodes in patients with type 1 diabetes. *Diabetes* **60,** 2903–2913 (2011).
36. Vecchione, A., Jofra, T., Gerosa, J., Shankwitz, K., Di Fonte, R., Galvani, G., Ippolito, E., Cicalese, M. P., Schultz, A. R., Seay, H. R., Favellato, M., Milardi, G., Stabilini, A., Ragogna, F., Grogan, P., Bianconi, E., Laurenzi, A., Caretto, A., Nano, R., Melzi, R., Danzl, N., Bosi, E., Piemonti, L., Aiuti, A., Brusko, T., Petrovas, C., Battaglia, M. & Fousteri, G. Reduced Follicular Regulatory T Cells in Spleen and Pancreatic Lymph Nodes of Patients With Type 1 Diabetes. *Diabetes* **70,** 2892–2902 (2021).
37. Kaestner, K. H., Powers, A. C., Naji, A., HPAP Consortium & Atkinson, M. A. NIH Initiative to Improve Understanding of the Pancreas, Islet, and Autoimmunity in Type 1 Diabetes: The Human Pancreas Analysis Program (HPAP). *Diabetes* **68,** 1394–1402 (2019).
38. Kliche, S., Breitling, D., Togni, M., Pusch, R., Heuer, K., Wang, X., Freund, C., Kasirer-Friede, A., Menasche, G., Koretzky, G. A. & Schraven, B. The ADAP/SKAP55 signaling module regulates T-cell receptor-mediated integrin activation through plasma membrane targeting of Rap1. *Mol. Cell. Biol.* **26,** 7130–7144 (2006).
39. Ferretti, A. P., Bhargava, R., Dahan, S., Tsokos, M. G. & Tsokos, G. C. Calcium/Calmodulin Kinase IV Controls the Function of Both T Cells and Kidney Resident Cells. *Front. Immunol.* **9,** 2113 (2018).

40. Fu, G., Hu, J., Niederberger-Magnenat, N., Rybakin, V., Casas, J., Yachi, P. P., Feldstein, S., Ma, B., Hoerter, J. A. H., Ampudia, J., Rigaud, S., Lambolez, F., Gavin, A. L., Sauer, K., Cheroutre, H. & Gascoigne, N. R. J. Protein kinase C η is required for T cell activation and homeostatic proliferation. *Sci. Signal.* **4,** ra84 (2011).
41. Kos, J., Nanut, M. P., Prunk, M., Sabotič, J., Dautović, E. & Jewett, A. Cystatin F as a regulator of immune cell cytotoxicity. *Cancer Immunol. Immunother.* **67,** 1931–1938 (2018).
42. O'Shea, J. J., Lahesmaa, R., Vahedi, G., Laurence, A. & Kanno, Y. Genomic views of STAT function in CD4+ T helper cell differentiation. *Nat. Rev. Immunol.* **11,** 239–250 (2011).
43. Readinger, J. A., Mueller, K. L., Venegas, A. M., Horai, R. & Schwartzberg, P. L. Tec kinases regulate T-lymphocyte development and function: new insights into the roles of Itk and Rlk/Txk. *Immunol. Rev.* **228,** 93–114 (2009).
44. Takeba, Y., Nagafuchi, H., Takeno, M., Kashiwakura, J.-I. & Suzuki, N. Txk, a member of nonreceptor tyrosine kinase of Tec family, acts as a Th1 cell-specific transcription factor and regulates IFN-gamma gene transcription. *J. Immunol.* **168,** 2365–2370 (2002).
45. Vella, A., Cooper, J. D., Lowe, C. E., Walker, N., Nutland, S., Widmer, B., Jones, R., Ring, S. M., McArdle, W., Pembrey, M. E., Strachan, D. P., Dunger, D. B., Twells, R. C. J., Clayton, D. G. & Todd, J. A. Localization of a type 1 diabetes locus in the IL2RA/CD25 region by use of tag single-nucleotide polymorphisms. *Am. J. Hum. Genet.* **76,** 773–779 (2005).
46. Grinberg-Bleyer, Y., Baeyens, A., You, S., Elhage, R., Fourcade, G., Gregoire, S., Cagnard, N., Carpentier, W., Tang, Q., Bluestone, J., Chatenoud, L., Klatzmann, D., Salomon, B. L. & Piaggio, E. IL-2 reverses established type 1 diabetes in NOD mice by a local effect on pancreatic regulatory T cells. *J. Exp. Med.* **207,** 1871–1878 (2010).
47. Ohkura, N. & Sakaguchi, S. Transcriptional and epigenetic basis of Treg cell development and function: its genetic anomalies or variations in autoimmune diseases. *Cell Res.* **30,** 465–474 (2020).
48. Shevyrev, D. & Tereshchenko, V. Treg Heterogeneity, Function, and Homeostasis. *Front. Immunol.* **10,** 3100 (2019).
49. Dowling, O., Difeo, A., Ramirez, M. C., Tukel, T., Narla, G., Bonafe, L., Kayserili, H., Yuksel-Apak, M., Paller, A. S., Norton, K., Teebi, A. S., Grum-Tokars, V., Martin, G. S., Davis, G. E., Glucksman, M. J. & Martignetti, J. A. Mutations in capillary morphogenesis gene-2 result in the allelic disorders juvenile hyaline fibromatosis and infantile systemic hyalinosis. *Am. J. Hum. Genet.* **73,** 957–966 (2003).
50. Li, J., Lu, E., Yi, T. & Cyster, J. G. EBI2 augments Tfh cell fate by promoting interaction with IL-2-quenching dendritic cells. *Nature* **533,** 110–114 (2016).
51. Lin, S.-E., Oyama, T., Nagase, T., Harigaya, K. & Kitagawa, M. Identification of new human mastermind proteins defines a family that consists of positive regulators for notch signaling. *J. Biol. Chem.* **277,** 50612–50620 (2002).
52. Ghosh, S., Roy-Chowdhuri, S., Kang, K., Im, S.-H. & Rudra, D. The transcription factor Foxp1 preserves integrity of an active Foxp3 locus in extrathymic Treg cells. *Nat. Commun.* **9,** 4473 (2018).
53. Ono, M., Yaguchi, H., Ohkura, N., Kitabayashi, I., Nagamura, Y., Nomura, T., Miyachi, Y., Tsukada, T. & Sakaguchi, S. Foxp3 controls regulatory T-cell function by interacting with AML1/Runx1. *Nature* **446,** 685–689 (2007).
54. Han, K., Singh, K., Rodman, M. J., Hassanzadeh, S., Wu, K., Nguyen, A., Huffstutler, R. D., Seifuddin, F., Dagur, P. K., Saxena, A., McCoy, J. P., Chen, J., Biancotto, A., Stagliano, K. E. R., Teague, H. L., Mehta, N. N., Pirooznia, M. & Sack, M. N. Fasting-induced FOXO4 blunts human CD4+ T helper cell responsiveness. *Nat Metab* **3,** 318–326 (2021).
55. Vacchio, M. S., Olaru, A., Livak, F. & Hodes, R. J. ATM deficiency impairs thymocyte maturation because of defective resolution of T cell receptor α locus coding end breaks. *Proceedings of the National Academy of Sciences* **104,** 6323–6328 (2007).
56. Ivetic, A., Hoskins Green, H. L. & Hart, S. J. L-selectin: A Major Regulator of Leukocyte Adhesion, Migration and Signaling. *Front. Immunol.* **10,** 1068 (2019).

57. Roychoudhuri, R., Clever, D., Li, P., Wakabayashi, Y., Quinn, K. M., Klebanoff, C. A., Ji, Y., Sukumar, M., Eil, R. L., Yu, Z., Spolski, R., Palmer, D. C., Pan, J. H., Patel, S. J., Macallan, D. C., Fabozzi, G., Shih, H.-Y., Kanno, Y., Muto, A., Zhu, J., Gattinoni, L., O'Shea, J. J., Okkenhaug, K., Igarashi, K., Leonard, W. J. & Restifo, N. P. BACH2 regulates CD8(+) T cell differentiation by controlling access of AP-1 factors to enhancers. *Nat. Immunol.* **17,** 851–860 (2016).
58. Yao, C., Lou, G., Sun, H.-W., Zhu, Z., Sun, Y., Chen, Z., Chauss, D., Moseman, E. A., Cheng, J., D'Antonio, M. A., Shi, W., Shi, J., Kometani, K., Kurosaki, T., Wherry, E. J., Afzali, B., Gattinoni, L., Zhu, Y., McGavern, D. B., O'Shea, J. J., Schwartzberg, P. L. & Wu, T. BACH2 enforces the transcriptional and epigenetic programs of stem-like CD8+ T cells. *Nat. Immunol.* **22,** 370–380 (2021).
59. Kanehisa, M. & Goto, S. KEGG: kyoto encyclopedia of genes and genomes. *Nucleic Acids Res.* **28,** 27–30 (2000).
60. Kanehisa, M. Toward understanding the origin and evolution of cellular organisms. *Protein Sci.* **28,** 1947–1951 (2019).
61. Kanehisa, M., Furumichi, M., Sato, Y., Kawashima, M. & Ishiguro-Watanabe, M. KEGG for taxonomy-based analysis of pathways and genomes. *Nucleic Acids Res.* **51,** D587–D592 (2023).
62. Boulland, M.-L., Marquet, J., Molinier-Frenkel, V., Möller, P., Guiter, C., Lasoudris, F., Copie-Bergman, C., Baia, M., Gaulard, P., Leroy, K. & Castellano, F. Human IL4I1 is a secreted L-phenylalanine oxidase expressed by mature dendritic cells that inhibits T-lymphocyte proliferation. *Blood* **110,** 220–227 (2007).
63. Pociot, F., Akolkar, B., Concannon, P., Erlich, H. A., Julier, C., Morahan, G., Nierras, C. R., Todd, J. A., Rich, S. S. & Nerup, J. Genetics of type 1 diabetes: what's next? *Diabetes* **59,** 1561–1571 (2010).
64. Noble, J. A. & Erlich, H. A. Genetics of type 1 diabetes. *Cold Spring Harb. Perspect. Med.* **2,** a007732 (2012).
65. Noble, J. A. & Valdes, A. M. Genetics of the HLA region in the prediction of type 1 diabetes. *Curr. Diab. Rep.* **11,** 533–542 (2011).
66. Johnson, M. B., Patel, K. A., De Franco, E., Hagopian, W., Killian, M., McDonald, T. J., Tree, T. I. M., Domingo-Vila, C., Hudson, M., Hammersley, S., Dobbs, R., EXE-T1D Consortium, Ellard, S., Flanagan, S. E., Hattersley, A. T. & Oram, R. A. Type 1 diabetes can present before the age of 6 months and is characterised by autoimmunity and rapid loss of beta cells. *Diabetologia* **63,** 2605–2615 (2020).
67. Oram, R. A., Patel, K., Hill, A., Shields, B., McDonald, T. J., Jones, A., Hattersley, A. T. & Weedon, M. N. A Type 1 Diabetes Genetic Risk Score Can Aid Discrimination Between Type 1 and Type 2 Diabetes in Young Adults. *Diabetes Care* **39,** 337–344 (2016).
68. Sharp, S. A., Rich, S. S., Wood, A. R., Jones, S. E., Beaumont, R. N., Harrison, J. W., Schneider, D. A., Locke, J. M., Tyrrell, J., Weedon, M. N., Hagopian, W. A. & Oram, R. A. Development and Standardization of an Improved Type 1 Diabetes Genetic Risk Score for Use in Newborn Screening and Incident Diagnosis. *Diabetes Care* **42,** 200–207 (2019).
69. Roncarolo, M. G., Zoppo, M., Bacchetta, R., Gabiano, C., Sacchetti, C., Cerutti, F. & Tovo, P. A. Interleukin-2 production and interleukin-2 receptor expression in children with newly diagnosed diabetes. *Clin. Immunol. Immunopathol.* **49,** 53–62 (1988).
70. Tomoda, T., Kurashige, T. & Taniguchi, T. Imbalance of the interleukin 2 system in children with IDDM. *Diabetologia* **37,** 476–482 (1994).
71. Malek, T. R. & Bayer, A. L. Tolerance, not immunity, crucially depends on IL-2. *Nat. Rev. Immunol.* **4,** 665–674 (2004).
72. Kalia, V. & Sarkar, S. Regulation of Effector and Memory CD8 T Cell Differentiation by IL-2-A Balancing Act. *Front. Immunol.* **9,** 2987 (2018).
73. Li, J., Zaslavsky, M., Su, Y., Guo, J., Sikora, M. J., van Unen, V., Christophersen, A., Chiou, S.-H., Chen, L., Li, J., Ji, X., Wilhelmy, J., McSween, A. M., Palanski, B. A., Mallajosyula, V. V. A., Bracey, N. A., Dhondalay, G. K. R., Bhamidipati, K., Pai, J., Kipp, L. B., Dunn, J. E., Hauser, S. L., Oksenberg, J. R., Satpathy, A. T., Robinson, W. H., Dekker, C. L., Steinmetz, L. M., Khosla, C., Utz, P. J., Sollid, L. M., Chien, Y.-H., Heath, J. R., Fernandez-Becker, N. Q., Nadeau, K. C., Saligrama, N. & Davis, M. M.

KIR+CD8+ T cells suppress pathogenic T cells and are active in autoimmune diseases and COVID-19. *Science* **376,** eabi9591 (2022).
74. Achenbach, P., Koczwara, K., Knopff, A., Naserke, H., Ziegler, A.-G. & Bonifacio, E. Mature high-affinity immune responses to (pro)insulin anticipate the autoimmune cascade that leads to type 1 diabetes. *J. Clin. Invest.* **114,** 589–597 (2004).
75. Carrette, F. & Surh, C. D. IL-7 signaling and CD127 receptor regulation in the control of T cell homeostasis. *Semin. Immunol.* **24,** 209–217 (2012).
76. Vignali, D. & Monti, P. Targeting Homeostatic T Cell Proliferation to Control Beta-Cell Autoimmunity. *Curr. Diab. Rep.* **16,** 40 (2016).
77. Szabo, P. A., Miron, M. & Farber, D. L. Location, location, location: Tissue resident memory T cells in mice and humans. *Sci Immunol* **4,** (2019).
78. Cibrián, D. & Sánchez-Madrid, F. CD69: from activation marker to metabolic gatekeeper. *Eur. J. Immunol.* **47,** 946–953 (2017).
79. Orban, T., Sosenko, J. M., Cuthbertson, D., Krischer, J. P., Skyler, J. S., Jackson, R., Yu, L., Palmer, J. P., Schatz, D., Eisenbarth, G. & Diabetes Prevention Trial-Type 1 Study Group. Pancreatic islet autoantibodies as predictors of type 1 diabetes in the Diabetes Prevention Trial-Type 1. *Diabetes Care* **32,** 2269–2274 (2009).
80. Li, B., Yang, C., Jia, G., Liu, Y., Wang, N., Yang, F., Su, R., Shang, Y. & Han, Y. Comprehensive evaluation of the effects of long-term cryopreservation on peripheral blood mononuclear cells using flow cytometry. *BMC Immunol.* **23,** 30 (2022).
81. Japp, A. S., Meng, W., Rosenfeld, A. M., Perry, D. J., Thirawatananond, P., Bacher, R. L., Liu, C., Gardner, J. S., HPAP Consortium, Atkinson, M. A., Kaestner, K. H., Brusko, T. M., Naji, A., Luning Prak, E. T. & Betts, M. R. TCR+/BCR+ dual-expressing cells and their associated public BCR clonotype are not enriched in type 1 diabetes. *Cell* **184,** 827–839.e14 (2021).
82. Kuri-Cervantes, L., Pampena, M. B. & Betts, M. R. Phenotypic Characterization of SLex+ and CLA+ CD4+ T Cells. *STAR Protoc* **1,** 100154 (2020).
83. Stoeckius, M., Hafemeister, C., Stephenson, W., Houck-Loomis, B., Chattopadhyay, P. K., Swerdlow, H., Satija, R. & Smibert, P. Simultaneous epitope and transcriptome measurement in single cells. *Nat. Methods* **14,** 865–868 (2017).
84. Stoeckius, M., Zheng, S., Houck-Loomis, B., Hao, S., Yeung, B. Z., Mauck, W. M., 3rd, Smibert, P. & Satija, R. Cell Hashing with barcoded antibodies enables multiplexing and doublet detection for single cell genomics. *Genome Biol.* **19,** 224 (2018).
85. Melsted, P., Booeshaghi, A. S., Liu, L., Gao, F., Lu, L., Min, K. H. J., da Veiga Beltrame, E., Hjörleifsson, K. E., Gehring, J. & Pachter, L. Modular, efficient and constant-memory single-cell RNA-seq preprocessing. *Nat. Biotechnol.* **39,** 813–818 (2021).
86. Korsunsky, I., Millard, N., Fan, J., Slowikowski, K., Zhang, F., Wei, K., Baglaenko, Y., Brenner, M., Loh, P.-R. & Raychaudhuri, S. Fast, sensitive and accurate integration of single-cell data with Harmony. *Nat. Methods* **16,** 1289–1296 (2019).
87. Seal, R. L., Braschi, B., Gray, K., Jones, T. E. M., Tweedie, S., Haim-Vilmovsky, L. & Bruford, E. A. Genenames.org: the HGNC resources in 2023. *Nucleic Acids Res.* **51,** D1003–D1009 (2023).
88. Langfelder, P. & Horvath, S. WGCNA: an R package for weighted correlation network analysis. *BMC Bioinformatics* **9,** 559 (2008).
89. Morabito, S., Reese, F., Rahimzadeh, N., Miyoshi, E. & Swarup, V. hdWGCNA identifies co-expression networks in high-dimensional transcriptomics data. *Cell Rep Methods* **3,** 100498 (2023).
90. Klitz, W., Maiers, M., Spellman, S., Baxter-Lowe, L. A., Schmeckpeper, B., Williams, T. M. & Fernandez-Viña, M. New HLA haplotype frequency reference standards: high-resolution and large sample typing of HLA DR-DQ haplotypes in a sample of European Americans. *Tissue Antigens* **62,** 296–307 (2003).
91. Hadley, W. *Ggplot2: Elegrant graphics for data analysis*. (Springer, 2016).

Figure 1

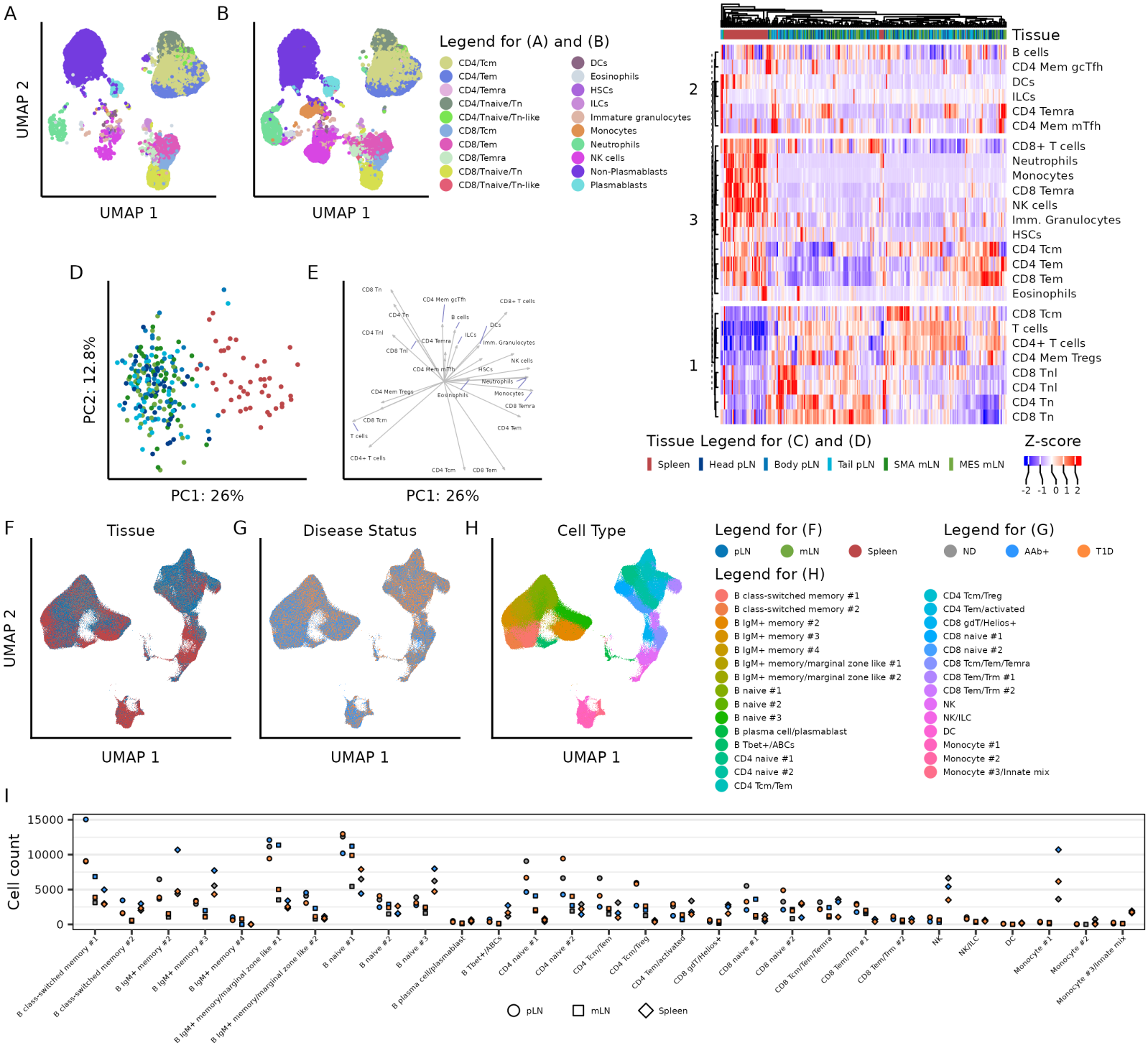
A
B
UMAP 2
UMAP 1
Legend for (A) and (B)
CD4/Tcm
CD4/Tem
CD4/Temra
CD4/Tnaive/Tn
CD4/Tnaive/Tn-like
CD8/Tcm
CD8/Tem
CD8/Temra
CD8/Tnaive/Tn
CD8/Tnaive/Tn-like
DCs
Eosinophils
HSCs
ILCs
Immature granulocytes
Monocytes
Neutrophils
NK cells
Non-Plasmablasts
Plasmablasts
C
Tissue
B cells
CD4 Mem gcTfh
DCs
ILCs
CD4 Temra
CD4 Mem mTfh
CD8+ T cells
Neutrophils
Monocytes
CD8 Temra
NK cells
Imm. Granulocytes
HSCs
CD4 Tcm
CD4 Tem
CD8 Tem
Eosinophils
CD8 Tcm
T cells
CD4+ T cells
CD4 Mem Tregs
CD8 Tnl
CD4 Tnl
CD4 Tn
CD8 Tn
2
3
1
Tissue Legend for (C) and (D)
Spleen
Head pLN
Body pLN
Tail pLN
SMA mLN
MES mLN
Z-score
-2 -1 0 1 2
D
PC2: 12.8%
PC1: 26%
E
PC1: 26%
F
Tissue
G
Disease Status
H
Cell Type
UMAP 2
UMAP 1
Legend for (F)
pLN
mLN
Spleen
Legend for (G)
ND
AAb+
T1D
Legend for (H)
B class-switched memory #1
B class-switched memory #2
B IgM+ memory #2
B IgM+ memory #3
B IgM+ memory #4
B IgM+ memory/marginal zone like #1
B IgM+ memory/marginal zone like #2
B naive #1
B naive #2
B naive #3
B plasma cell/plasmablast
B Tbet+/ABCs
CD4 naive #1
CD4 naive #2
CD4 Tcm/Tem
CD4 Tcm/Treg
CD4 Tem/activated
CD8 gdT/Helios+
CD8 naive #1
CD8 naive #2
CD8 Tcm/Tem/Temra
CD8 Tem/Trm #1
CD8 Tem/Trm #2
NK
NK/ILC
DC
Monocyte #1
Monocyte #2
Monocyte #3/Innate mix
I
Cell count
15000
10000
5000
0
pLN
mLN
Spleen

Figure 2

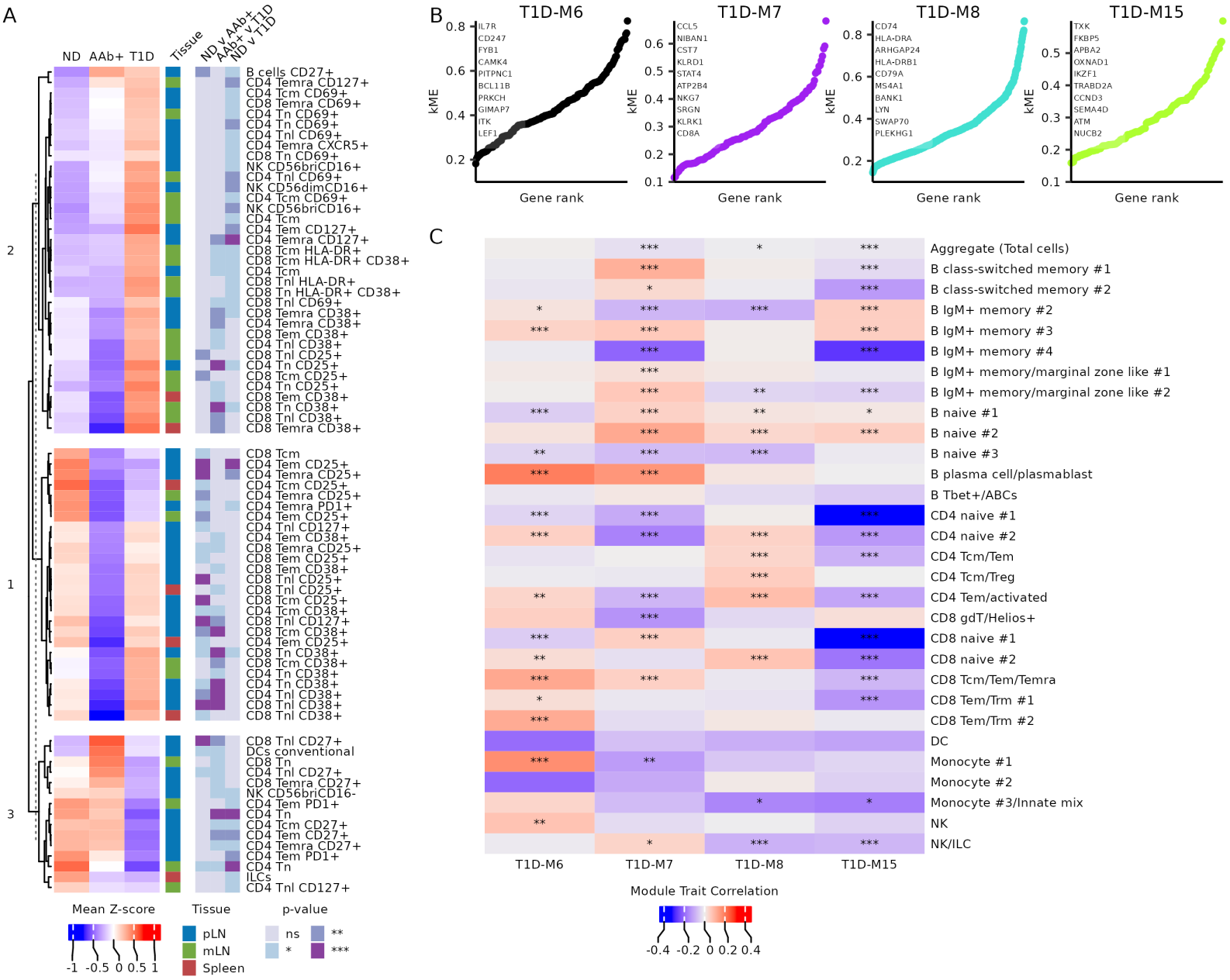
A
ND AAb+ T1D
Tissue
ND v AAb+
AAb+ v T1D
ND v T1D
B cells CD27+
CD4 Temra CD127+
CD4 Tcm CD69+
CD8 Temra CD69+
CD4 Tn CD69+
CD4 Tn CD69+
CD4 Tnl CD69+
CD4 Temra CXCR5+
CD8 Tn CD69+
NK CD56briCD16+
CD4 Tnl CD69+
NK CD56dimCD16+
CD4 Tcm CD69+
NK CD56briCD16+
CD4 Tcm
CD4 Tem CD127+
CD4 Temra CD127+
CD8 Tcm HLA-DR+
CD8 Tcm HLA-DR+ CD38+
CD4 Tcm
CD8 Tnl HLA-DR+
CD8 Tn HLA-DR+ CD38+
CD8 Tnl CD69+
CD8 Temra CD38+
CD4 Temra CD38+
CD8 Tem CD38+
CD4 Tnl CD38+
CD8 Tnl CD25+
CD4 Tn CD25+
CD8 Tcm CD25+
CD4 Tn CD25+
CD8 Tem CD38+
CD8 Tn CD38+
CD8 Tnl CD38+
CD8 Temra CD38+
CD8 Tcm
CD4 Tem CD25+
CD4 Temra CD25+
CD4 Tcm CD25+
CD4 Temra CD25+
CD4 Temra PD1+
CD4 Tem CD25+
CD4 Tnl CD127+
CD4 Tem CD38+
CD8 Temra CD25+
CD8 Tem CD25+
CD8 Tem CD38+
CD8 Tnl CD25+
CD8 Tnl CD25+
CD8 Tcm CD25+
CD4 Tcm CD38+
CD8 Tnl CD127+
CD8 Tcm CD38+
CD4 Tem CD25+
CD8 Tn CD38+
CD8 Tcm CD38+
CD4 Tn CD38+
CD4 Tn CD38+
CD4 Tnl CD38+
CD8 Tnl CD38+
CD8 Tnl CD38+
CD8 Tnl CD27+
DCs conventional
CD8 Tn
CD4 Tnl CD27+
CD8 Temra CD27+
NK CD56briCD16-
CD4 Tem PD1+
CD4 Tn
CD4 Tcm CD27+
CD4 Tem CD27+
CD4 Temra CD27+
CD4 Tem PD1+
CD4 Tn
ILCs
CD4 Tnl CD127+
1
2
3
Mean Z-score
-1 -0.5 0 0.5 1
Tissue
pLN
mLN
Spleen
p-value
ns
*
**
***
B
T1D-M6
T1D-M7
T1D-M8
T1D-M15
kME
Gene rank
IL7R
CD247
FYB1
CAMK4
PITPNC1
BCL11B
PRKCH
GIMAP7
ITK
LEF1
CCL5
NIBAN1
CST7
KLRD1
STAT4
ATP2B4
NKG7
SRGN
KLRK1
CD8A
CD74
HLA-DRA
ARHGAP24
HLA-DRB1
CD79A
MS4A1
BANK1
LYN
SWAP70
PLEKHG1
TXK
FKBP5
APBA2
OXNAD1
IKZF1
TRABD2A
CCND3
SEMA4D
ATM
NUCB2
C
Aggregate (Total cells)
B class-switched memory #1
B class-switched memory #2
B IgM+ memory #2
B IgM+ memory #3
B IgM+ memory #4
B IgM+ memory/marginal zone like #1
B IgM+ memory/marginal zone like #2
B naive #1
B naive #2
B naive #3
B plasma cell/plasmablast
B Tbet+/ABCs
CD4 naive #1
CD4 naive #2
CD4 Tcm/Tem
CD4 Tcm/Treg
CD4 Tem/activated
CD8 gdT/Helios+
CD8 naive #1
CD8 naive #2
CD8 Tcm/Tem/Temra
CD8 Tem/Trm #1
CD8 Tem/Trm #2
DC
Monocyte #1
Monocyte #2
Monocyte #3/Innate mix
NK
NK/ILC
T1D-M6
T1D-M7
T1D-M8
T1D-M15
Module Trait Correlation
-0.4 -0.2 0 0.2 0.4

Figure 3

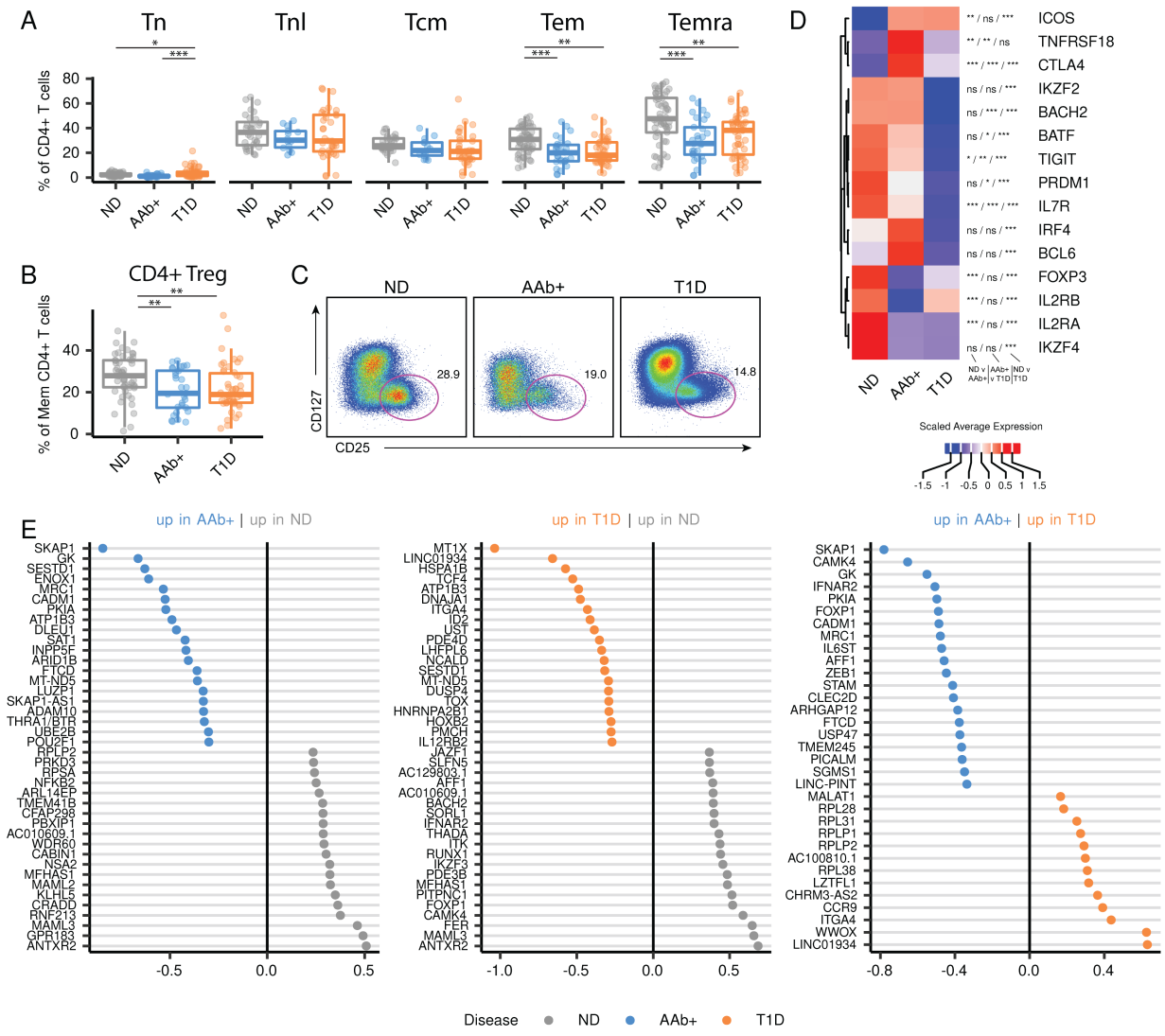
A
Tn
Tnl
Tcm
Tem
Temra
% of CD4+ T cells
ND
AAb+
T1D
B
CD4+ Treg
% of Mem CD4+ T cells
C
ND
AAb+
T1D
CD127
CD25
28.9
19.0
14.8
D
ICOS
TNFRSF18
CTLA4
IKZF2
BACH2
BATF
TIGIT
PRDM1
IL7R
IRF4
BCL6
FOXP3
IL2RB
IL2RA
IKZF4
Scaled Average Expression
E
up in AAb+ | up in ND
up in T1D | up in ND
up in AAb+ | up in T1D
Disease
ND
AAb+
T1D

Figure 4

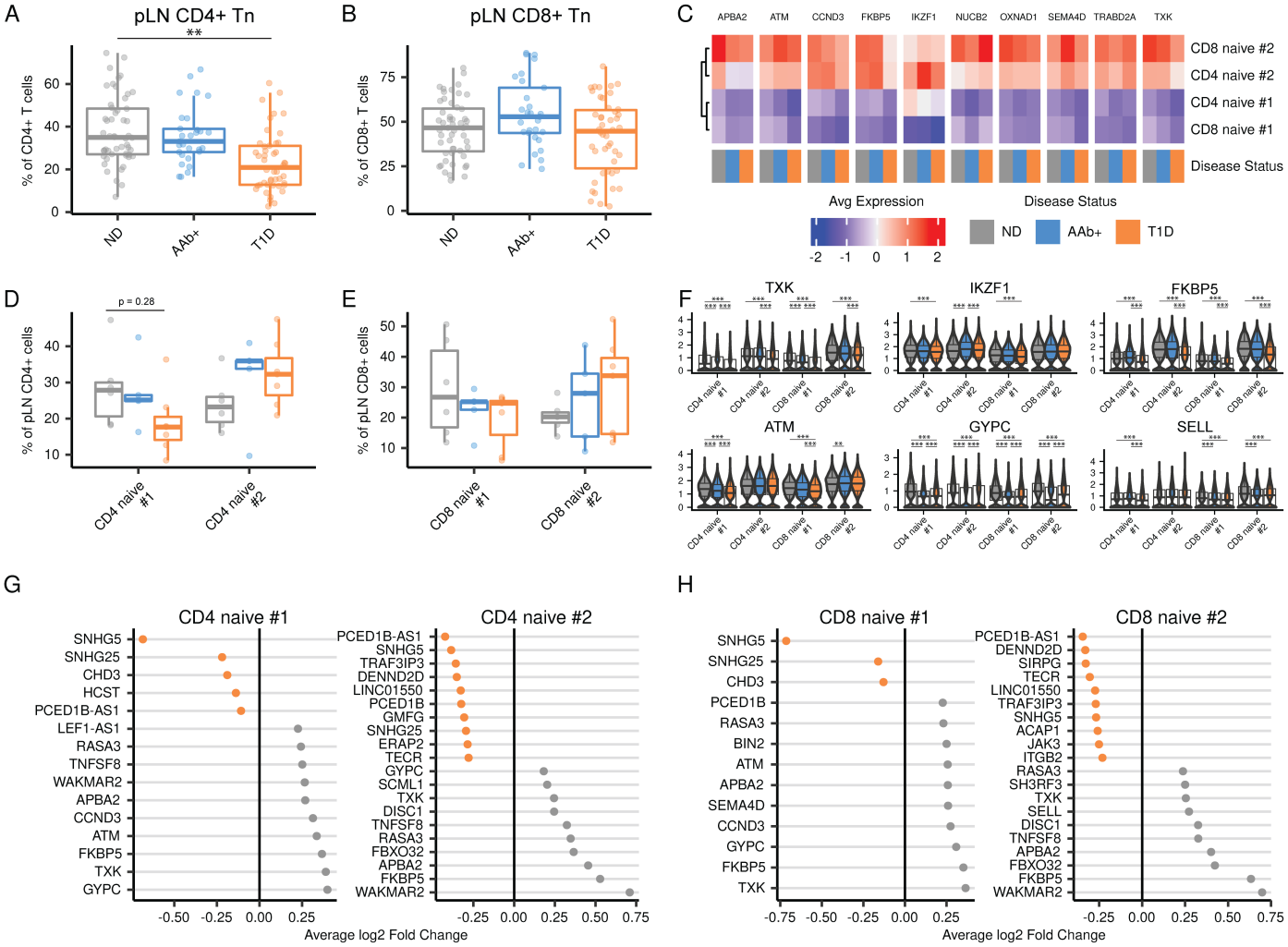
A
pLN CD4+ Tn
**
% of CD4+ T cells
ND
AAb+
T1D
B
pLN CD8+ Tn
% of CD8+ T cells
C
APBA2
ATM
CCND3
FKBP5
IKZF1
NUCB2
OXNAD1
SEMA4D
TRABD2A
TXK
CD8 naive #2
CD4 naive #2
CD4 naive #1
CD8 naive #1
Disease Status
Avg Expression
Disease Status
ND
AAb+
T1D
D
p = 0.28
% of pLN CD4+ cells
CD4 naive #1
CD4 naive #2
E
% of pLN CD8+ cells
CD8 naive #1
CD8 naive #2
F
TXK
IKZF1
FKBP5
ATM
GYPC
SELL

G
CD4 naive #1
SNHG5
SNHG25
CHD3
HCST
PCED1B-AS1
LEF1-AS1
RASA3
TNFSF8
WAKMAR2
APBA2
CCND3
ATM
FKBP5
TXK
GYPC
CD4 naive #2
PCED1B-AS1
SNHG5
TRAF3IP3
DENND2D
LINC01550
PCED1B
GMFG
SNHG25
ERAP2
TECR
GYPC
SCML1
TXK
DISC1
TNFSF8
RASA3
FBXO32
APBA2
FKBP5
WAKMAR2
Average log2 Fold Change
H
CD8 naive #1
SNHG5
SNHG25
CHD3
PCED1B
RASA3
BIN2
ATM
APBA2
SEMA4D
CCND3
GYPC
FKBP5
TXK
CD8 naive #2
PCED1B-AS1
DENND2D
SIRPG
TECR
LINC01550
TRAF3IP3
SNHG5
ACAP1
JAK3
ITGB2
RASA3
SH3RF3
TXK
SELL
DISC1
TNFSF8
APBA2
FBXO32
FKBP5
WAKMAR2
Average log2 Fold Change

Figure 5

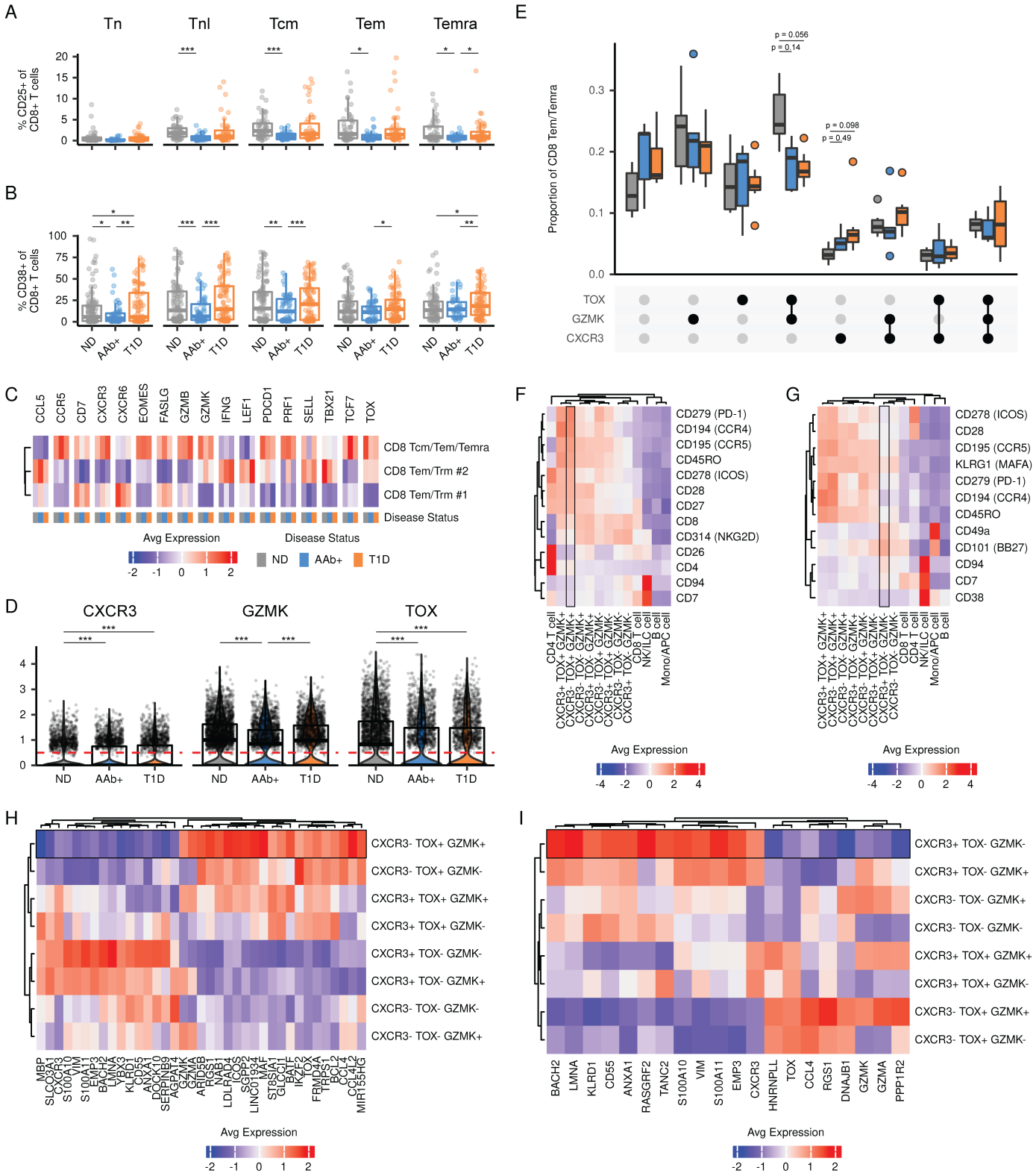

A
Tn
Tnl
Tcm
Tem
Temra
% CD25+ of CD8+ T cells
B
% CD38+ of CD8+ T cells
ND
AAb+
T1D
C
CCL5
CCR5
CD7
CXCR3
CXCR6
EOMES
FASLG
GZMB
GZMK
IFNG
LEF1
PDCD1
PRF1
SELL
TBX21
TCF7
TOX
CD8 Tcm/Tem/Temra
CD8 Tem/Trm #2
CD8 Tem/Trm #1
Disease Status
Avg Expression
Disease Status
ND
AAb+
T1D
D
CXCR3
GZMK
TOX
E
Proportion of CD8 Tem/Temra
p = 0.056
p = 0.14
p = 0.098
p = 0.49
TOX
GZMK
CXCR3
F
CD279 (PD-1)
CD194 (CCR4)
CD195 (CCR5)
CD45RO
CD278 (ICOS)
CD28
CD27
CD8
CD314 (NKG2D)
CD26
CD4
CD94
CD7
Avg Expression
G
CD278 (ICOS)
CD28
CD195 (CCR5)
KLRG1 (MAFA)
CD279 (PD-1)
CD194 (CCR4)
CD45RO
CD49a
CD101 (BB27)
CD94
CD7
CD38
Avg Expression
H
CXCR3- TOX+ GZMK+
CXCR3- TOX+ GZMK-
CXCR3+ TOX+ GZMK+
CXCR3+ TOX+ GZMK-
CXCR3+ TOX- GZMK-
CXCR3+ TOX- GZMK+
CXCR3- TOX- GZMK-
CXCR3- TOX- GZMK+
Avg Expression
I
CXCR3+ TOX- GZMK-
CXCR3+ TOX- GZMK+
CXCR3- TOX- GZMK+
CXCR3- TOX- GZMK-
CXCR3+ TOX+ GZMK+
CXCR3+ TOX+ GZMK-
CXCR3- TOX+ GZMK+
CXCR3- TOX+ GZMK-
Avg Expression

Figure 6

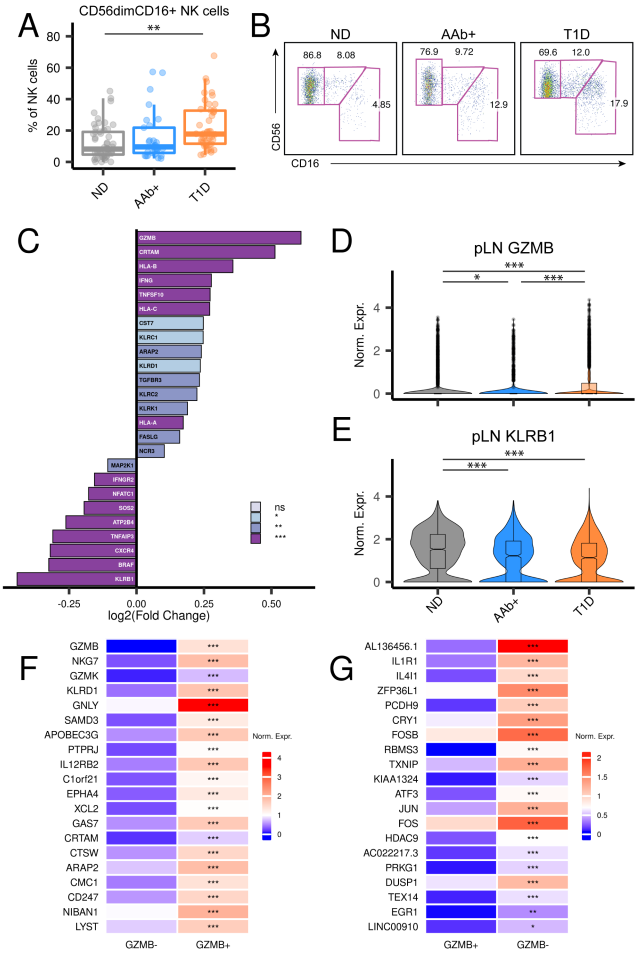
A
CD56dimCD16+ NK cells
% of NK cells
ND
AAb+
T1D
B
ND
AAb+
T1D
86.8
8.08
4.85
76.9
9.72
12.9
69.6
12.0
17.9
CD56
CD16
C
log2(Fold Change)
D
pLN GZMB
Norm. Expr.
E
pLN KLRB1
Norm. Expr.
F
Norm. Expr.
GZMB-
GZMB+
G
Norm. Expr.
GZMB+
GZMB-

Figure 7

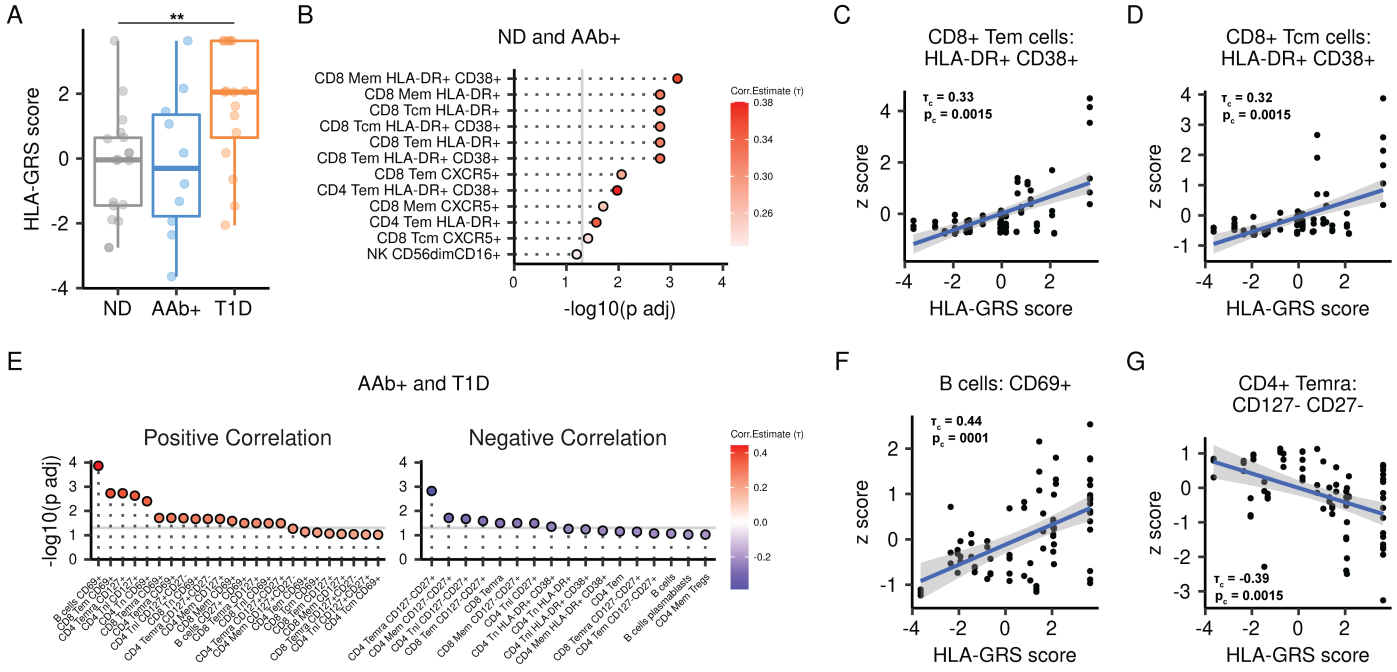
A
**
HLA-GRS score
ND
AAb+
T1D
B
ND and AAb+
CD8 Mem HLA-DR+ CD38+
CD8 Mem HLA-DR+
CD8 Tcm HLA-DR+
CD8 Tcm HLA-DR+ CD38+
CD8 Tem HLA-DR+
CD8 Tem HLA-DR+ CD38+
CD8 Tem CXCR5+
CD4 Tem HLA-DR+ CD38+
CD8 Mem CXCR5+
CD4 Tem HLA-DR+
CD8 Tcm CXCR5+
NK CD56dimCD16+
-log10(p adj)
Corr.Estimate (τ)
C
CD8+ Tem cells:
HLA-DR+ CD38+
τc = 0.33
pc = 0.0015
z score
HLA-GRS score
D
CD8+ Tcm cells:
HLA-DR+ CD38+
τc = 0.32
pc = 0.0015
z score
HLA-GRS score
E
AAb+ and T1D
Positive Correlation
Negative Correlation
-log10(p adj)
Corr.Estimate (τ)
F
B cells: CD69+
τc = 0.44
pc = 0001
z score
HLA-GRS score
G
CD4+ Temra:
CD127- CD27-
τc = -0.39
pc = 0.0015
z score
HLA-GRS score